A NUMERICAL SOLUTION FOR THE FLOW FIELD OF A SUPERSONIC CONE-CYLINDER ENTERING AND LEAVING A BLAST SPHERE DIAMETRICALLY

By

ROGER RALPH EATON

Bachelor of Science
Kansas State University
Manhattan, Kansas
1960

Master of Science
Kansas State University
Manhattan, Kansas
1962

Submitted to the Faculty of the Graduate School
of the Oklahoma State University
in partial fulfillment of the requirements
for the degree of
DOCTOR OF PHILOSOPHY
May, 1967

A NUMERICAL SOLUTION FOR THE FLOW FIELD OF
A SUPERSONIC CONE-CYLINDER ENTERING AND
LEAVING A BLAST SPHERE DIAMETRICALLY

Thesis Approved:

G W Zumwalt
Thesis Adviser

Ladislaus J Fila

Karl N. Reid

Dale D. Grosvenor

N D Durham
Dean of the Graduate College

PREFACE

A study was undertaken in which the flow properties about a cone-cylinder configuration were approximated for two different transient conditions of interest, those of entering and exiting diametrically from a spherical blast of large radius. A complete case was computed for ideal gas and equilibrium real gas.

This work was completed under the sponsorship of Sandia Corporation, Albuquerque, New Mexico, and constitutes a single segment in the overall program of developing the capability of predicting phenomena which occur when a blast wave and a ballistic vehicle intersect. Three associated studies at Oklahoma State University preceded this undertaking; all three used numerical techniques. Dr. L. D. Tyler studied a plane shock as it emerged into both still and supersonic streams; Dr. W. N. Jackomis considered the transient flow field resulting from a blast wave intercepting a stationary cone; and Dr. W. F. Walker devised a method whereby the interaction of a moving shock wave with a turbulent mixing region could be studied.

Investigations into other aspects of the blast intercept problem are presently being conducted at Oklahoma State University under the Sandia contract. Mr. R. J. Damkevala is undertaking a laboratory experiment in which a supersonic projectile will be photographed as it is intercepted from the side by a blast front, and Captain J. J. Prentice is studying the flow phenomena about a sharp cone at an angle of attack.

My sincere appreciation is extended to the following individuals: Dr. G. W. Zumwalt, who served as my major thesis adviser and graduate committee chairman - his encouragement, guidance, and project financial support were invaluable during my graduate study; Professor L. J. Fila, who gave many hours of his time to discuss the various facets of the problem, and whose comments and suggestions were of great help; Dr. D. D. Grosvenor and Dr. K. N. Reid for serving on my graduate committee.

I would also like to thank the Sandia Corporation for their project financial help; the National Aeronautics and Space Administration for my NASA Trainee Fellowship; the University Computer Center, under the direction of Dr. D. D. Grosvenor; Mr. William Accola, a member of the computing staff; and Mr. Leonard McCommon for the drafting; finally, my wife, Donna, for giving up her job as a technical staff member at Sandia Corporation and returning to the status of a student's wife, and also for her direct help in the capacity of a computer programmer, in typing rough drafts, and in proofreading the manuscript.

TABLE OF CONTENTS

LIST OF TABLES

LIST OF FIGURES

NOMENCLATURE

$A(r,z,t)$	blurring term coefficient for z-direction
$B(r,z,t)$	blurring term coefficient for r-direction
c	local sonic velocity
e	fluid energy per unit volume
f	space sensitive function (completely defined on page 13)
F^r	space sensitive function (completely defined on page 13)
F^z	space sensitive function (completely defined on page 13)
h	diagonal of finite mesh
h_1	finite mesh spacing in z-direction
h_2	finite mesh spacing in r-direction
I	m location of nose for sharp cone
K	time parameter defined on page 17
K_1	time parameter defined on page 17
K_2	time parameter defined on page 17
ℓ	mesh number in r-direction (at $r = 0$, $\ell = 1$)
m	mesh number in z-direction (at $z = 0$, $m = 1$)
M	Mach number
n	time plane number
N	maximum number of mesh points in z-direction
p	static pressure

P	dimensionless pressure
r	coordinate perpendicular to cone axis
R	polar distance from origin
RHO	dimensionless density
RM	dimensionless r-mass flux
t	time
TP	time plane
u	velocity in z-direction
U	dimensionless velocity in z-direction
v	velocity in r-direction
V	dimensionless velocity in r-direction
$\overline{V}$	total velocity vector
w	velocity modulus, $\sqrt{u^2 + v^2}$
x	coordinate parallel to cone-cylinder axis of symmetry
y	coordinate perpendicular to cone-cylinder axis of symmetry
z	coordinate parallel to cone-cylinder axis of symmetry
ZM	dimensionless z-mass flux
α	coefficient of the "dissipative" difference term
β	coefficient of the "dissipative" difference term
γ	specific heat ratio
ϵ	energy (ergs/gram)
η	abscissa of rotated coordinate system
θ	R-coordinate angle measured from z-axis
ρ	density

σ	Courant number
τ	time increment
Φ	angle measured around axis of symmetry (z)
χ	cone half apex angle
ψ	defined on page 13
ω	stability constant

SUPERSCRIPTS

$\sim$	denotes terms which must be evaluated using property components along the (η, Φ) coordinates
n	time plane number
$'$	transformed plane where shock velocity = 0
s	quantities which relate to normal shock

SUBSCRIPTS

ℓ	r-net point location
m	z-net point location
o	standard atmosphere
1	region surrounding cone-cylinder during Phase 1
2	region left of normal shock initially existing in Phase 1
3	region left of normal shock initially existing in Phase 2
4	region left of normal shock initially existing in Phase 3

CHAPTER I

INTRODUCTION

In order to know and understand the flow field about a cone-cylinder as it enters and leaves a large spherical blast diametrically, it is necessary to study the two processes which occur as a projectile enters or exits axially through a plane blast front. By this study loads on the cone-cylinder may be calculated. These loads, in turn, can be used to specify the design shape of future cone-cylinders.

The configuration to be studied for the entering case is shown in Figure 1. Sketch "a" illustrates the cone-cylinder approaching the shock from the low pressure, undisturbed atmosphere; sketch "b" shows the cone in the process of entering the shock front; and sketch "c" indicates the new steady-state condition within the blast sphere.

Figure 2a shows the cone-cylinder approaching the shock from the high pressure side within the blast sphere. The projectile during its transient exiting state is illustrated by Figure 2b. Sketch "c" of Figure 2 shows the new steady-state condition in the undisturbed atmosphere.

The only study made previously on a similar configuration (cone-forebody) in this environment was made by W. S. Wolff (1). He only suggested the phenomena that might occur, but did not extend his study to a complete analysis. A complete study of the problem has not been

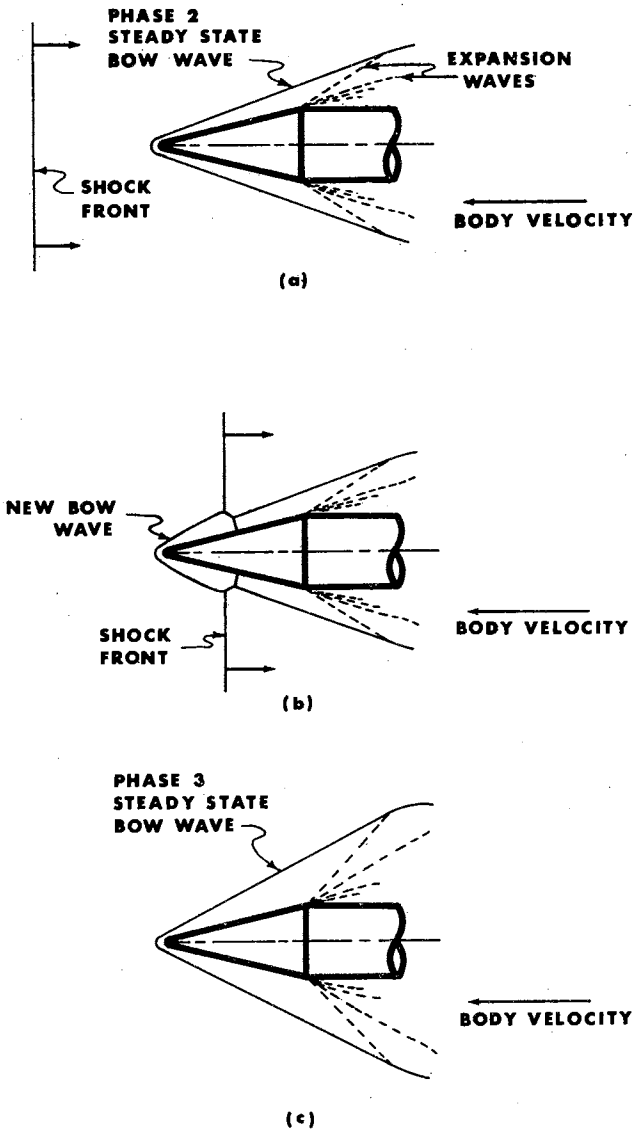

Figure 1. Progression of a Cone-Cylinder Entering a Blast Sphere

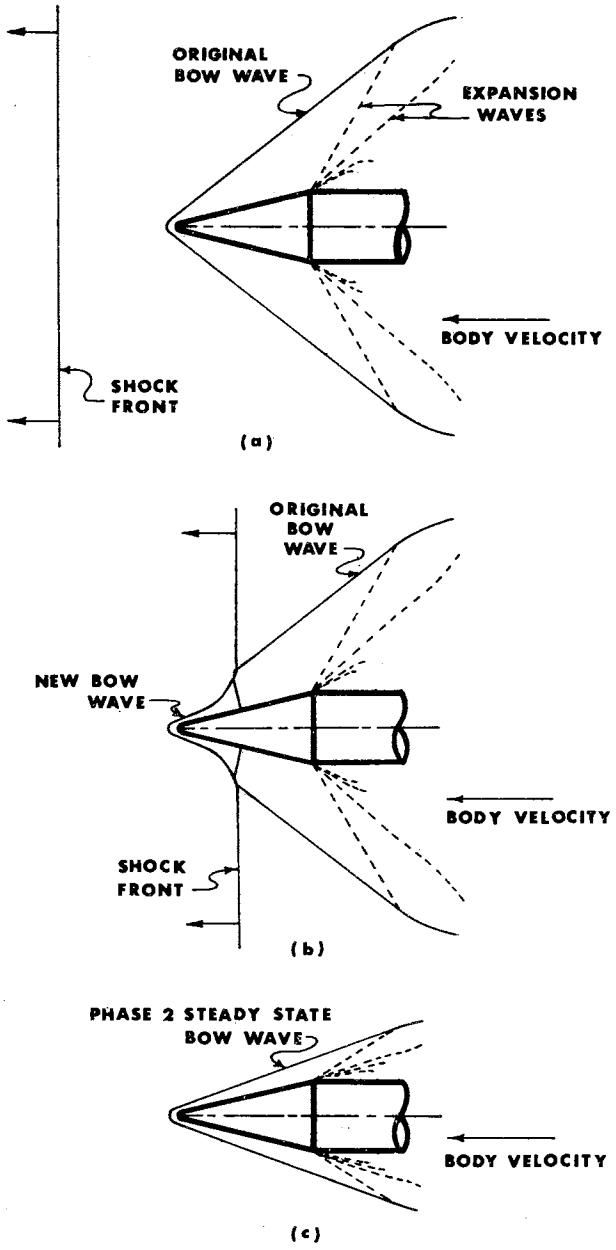

Figure 2. Progression of a Cone-Cylinder Exiting From a Blast Sphere

previously undertaken because of the difficulties involved in solving the controlling flow equations which are quasi-linear partial differential equations. Recently developed numerical techniques make it possible to approximate the solutions of the flow equations for transient and steady states. Many of these finite difference schemes use a mathematical "viscosity". This "viscosity" or blurring term allows a shock to be represented as a steep continuous gradient of properties rather than as a discontinuity. The gradients can then be handled numerically. These methods stem from the original work of J. von Neumann and R. D. Richtmyer (2).

The particular method used in this paper, which has been previously applied to other configurations, was developed by V. V. Rusanov (3). Tyler (4) applied it to a shock propagating into a cross flow; Jackomis (5) used it to describe the flow at the downstream blunt end of a cone; Walker (6) applied the method, with the addition of turbulent viscous terms, to a turbulent mixing region. None of the previous studies contains a stagnation point, nor do they have a bow shock existing in their steady-state field. However, this paper incorporates the above features, as well as a transient shock-on-shock and real gas effects; references (3) through (6) have been done for ideal gas only.

The study was divided into three phases. Phase 1 establishes a steady-state bow shock over a cone-cylinder configuration, which provides the initial data for Phase 2. Phase 2 consists of passing the cone from a high pressure, low velocity region into a low pressure, high velocity region, simulating the exiting of the body from a large diameter blast. Part 3 uses the steady-state flow field of Phase 2 for initial data.

The cone-cylinder is passed, during Phase 3, from the high velocity, low pressure region to a higher velocity, high pressure region. This simulates the entering of a projectile into a blast sphere from the undisturbed atmosphere.

The phases were computed in numerical order. Thus, the exiting problem was computed prior to the entering problem. This sequence was chosen so that the steady state obtained from the exiting case, Phase 2, could be used as initial data for the entering case, Phase 3. Consequently, the number of asymptotically approached steady-state solutions required were only three, whereas the enter-exit sequence would have required four.

CHAPTER II

LITERATURE SURVEY

The analysis of the reference material used in this study is presented in three sections: analytical, numerical, and experimental. Almost all discussed works deal with shock waves interacting with cones or wedges. A complete listing of related studies can be found in Walker and Tyler (7) or Tyler (4).

Analytical

Lighthill (8) considered the behavior of a plane shock wave, which was initially at rest with respect to the surrounding air, progressing along a wall and intersecting a small angle corner. Chester (9) extended the problem to the case of an infinite wedge at an angle of attack. By using the assumption that the shock meets the boundary nearly perpendicularly, he obtained a linearized solution of the pressure field. Extending the work of both Chester and Lighthill, Smyrl (10) found the pressure field, in closed analytical form, for the region behind an arbitrary plane shock which encountered a thin airfoil moving at supersonic speed. The problem which Smyrl linearized contained a new aspect, that of a contact discontinuity resulting from the shock collision.

The transient pressure field behind a plane shock wave of arbitrary strength which encounters a slender supersonic cone head-on was

theoretically predicted by Blankenship (11) by using a coordinate system for which time independent solutions for cones applied. The controlling flow equations were linearized in a manner similar to Smyrl's (10). The resulting system was solved iteratively by the method of successive over-relaxation, employing a relaxation factor to accelerate convergence.

Whitham (12), (13), and (14) developed an approximate theory for the prediction of shock patterns associated with the interaction of a blast wave with two-dimensional (plane and axi-symmetric) stationary bodies. Essentially based on kinematics considerations, the theory predicts only the shock wave patterns. Whitham's study did not yield the pressure distribution over the diffracted body, nor the flow field following the shock, and did not predict the shape or curvature of reflected shocks. Miles (15) extended Whitham's treatment of shock-shock diffraction to the diffraction of a shock wave moving into a region of uniform flow; the pressure profiles were also found. The results were applied to the diffraction of a blast wave by a thin wedge traveling at supersonic speed; and the pressures on the wedge immediately behind the blast wave were compared with those inferred from a complete solution of the boundary-value problem, Smyrl (10). Miles' method is considered to be approximate and Smyrl's exact; the results compare quantitatively.

The flight conditions analyzed by Wolff (1) are more similar to the conditions considered in this paper than any previous study. Wolff's work included the case of a cone forebody entering a spherical blast. He analyzed several types of interaction by assuming that the incident and reflected shock waves form a triangular pattern which grows with

time in a self-similar manner. Therefore, by a suitable translation of coordinates, the triangular shock pattern could be treated as a locally steady flow. Some discussion was also given for the cone leaving the blast sphere.

Numerical

Tyler (4) reported on the history of the development of numerical techniques. His work will not be duplicated here; instead, only articles appearing in the literature since May, 1965, and earlier articles not mentioned by Tyler will be discussed.

Burstein (16) calculated the steady hypersonic inviscid flow, including a detached shock around a blunt cylinder. The steady-state condition was obtained from the limit of the time dependent equations. Stable calculations were achieved by adding artificial viscosity terms and a solution was obtained using a variant of Richtmyer's two-step version of the Lax-Wendroff difference scheme.

A survey of numerical solutions of problems in gas dynamics, obtained in recent years in the U.S.S.R. with the aid of high-speed electronic computers, was presented by Maurice Holt (17). Brief discussions of some of the works of von Neumann, Richtmyer, Godunov, Okhotsimekil, Vlasova, and Rusanov were given.

Richtmyer (18) described several finite-difference approximations to the hyperbolic equations of fluid dynamics, and their qualities were assessed. Richtmyer's discussion included the schemes normally used and, for comparison, unstable and completely stable implicit schemes. Accuracy and stability were discussed. The Lax-Wendroff method, for a

system of conservation laws, was considered for problems in one and two space variables.

Gary (19) applied two finite difference techniques of second order accuracy, the Lax-Wendroff and iterative methods, to the equations of viscid and inviscid flow. An empirical stability criterion was obtained for the Lax-Wendroff scheme as applied to viscid flow. A stability criterion was obtained for the iterative method of von Neumann. The accuracy of these methods and their effectiveness for flows which contain a shock are also discussed by Gary.

Experimental

Several experimental studies have been undertaken to describe the transient flow that exists over cones and wedges which are intersected by shock fronts. In some cases the intersected body was initially stationary with respect to the surrounding air, while in others, the body progressed at a supersonic speed, opposite in direction to the shock front. The latter cases simulate the entering phase (Phase 3) of Chapter I. No experimental work has been done for the exiting phase (Phase 2).

Merritt and Aronson (20) studied the head-on interaction between a 9 degree cone in supersonic flight and a moving shock wave. Models, launched in a ballistics range with a 40 millimeter smooth bore powder gun, were flown into a shock front. A sequence of photographs of the interaction were taken through windows in the shock tube wall. Both model and shock wave Mach numbers were varied from two to five.

An experimental analysis of the axisymmetric case (head-on

interaction with a cone) was carried out by Brown and Mullaney (21) for slender bodies by conducting a series of tests using a 0.300 caliber gun-launched cone-cylinder model interacting with a plane shock wave generated by a conventional shock tube. Cones of 10 degrees and 20 degrees were fired into the shock front at 4000 and 3700 feet per second, respectively. In a companion article, Brown and Mullaney (22) analyzed the photographic results obtained in (21) with the use of the work done by Smyrl (10).

Bryson and Gross (23) presented experimental results of shock diffractions by several cones with different apex angles at shock Mach numbers between 3.5 and 4.0. The work was performed at Harvard University in air in a 4 inch x 12 inch x 40 feet shock tube. The experimental results were compared with the numerical results of Whitham's analytical studies.

Klein (24) used the hydraulic analogy to compressible gas flow for two-dimensional flow patterns to study the interaction of a shock wave and a wedge. Cases were run for both strong and weak shocks striking a wedge which was either in supersonic motion or stationary. The results were compared with the analytical results previously obtained by Smyrl (10).

Although several analytical, experimental, and numerical studies have been completed for cones and wedges in different phases of flight, no study has been made of a cone-cylinder configuration exiting from a blast using either numerical techniques or experiment, and the entering-the-blast case has been done only experimentally and by approximate analytical methods.

After studying the numerical procedures available, it was concluded that the method of Rusanov (3) would be most applicable for application to the exiting-entering problem. Based on Walker's (6) findings all transient shocks appearing in the flow field are more confined by Rusanov's method than other similar numerical techniques.

CHAPTER III

GOVERNING DIFFERENTIAL EQUATIONS

The governing axi-symmetric flow equations in a conservation form are:

Continuity,

$$\frac{\partial \rho}{\partial t} + \frac{\partial(\rho u)}{\partial z} + \frac{\partial(\rho v)}{\partial r} + \frac{\rho v}{r} = 0; \tag{3-1}$$

z-momentum,

$$\frac{\partial(\rho u)}{\partial t} + \frac{\partial(p+\rho u^2)}{\partial z} + \frac{\partial(\rho uv)}{\partial r} + \frac{\rho uv}{r} = 0; \tag{3-2}$$

r-momentum,

$$\frac{\partial(\rho v)}{\partial t} + \frac{\partial(\rho uv)}{\partial z} + \frac{\partial(p+\rho v^2)}{\partial r} + \frac{\rho v^2}{r} = 0; \tag{3-3}$$

Energy,

$$\frac{\partial e}{\partial t} + \frac{\partial(e+p)u}{\partial z} + \frac{\partial(e+p)v}{\partial r} + \frac{(e+p)v}{r} = 0. \tag{3-4}$$

Also required is a relationship between energy and pressure. This equation for ideal gas is,

$$e = \frac{p}{\gamma-1} + \frac{\rho|\bar{V}|^2}{2}. \tag{3-5}$$

The derivation of these equations can be found in reference (4), Tyler. Equations (3-1) through (3-4) are identical in form and can be written

$$\frac{\partial f}{\partial t} + \frac{\partial F^z}{\partial z} + \frac{\partial F^r}{\partial r} + \psi = 0,$$

where f, F^z, F^r, and ψ for the four equations, respectively, are

$$f = \begin{pmatrix} \rho \\ \rho u \\ \rho v \\ e \end{pmatrix}, \quad F^z = \begin{pmatrix} \rho u \\ p+\rho u^2 \\ \rho uv \\ (e+p)u \end{pmatrix}, \quad F^r = \begin{pmatrix} \rho v \\ \rho uv \\ p+\rho v^2 \\ (e+p)v \end{pmatrix}, \quad \psi = \frac{v}{r}\begin{pmatrix} \rho \\ \rho u \\ \rho v \\ e+p \end{pmatrix}. \quad (3\text{-}6)$$

The restrictions required by the above flow equations are:

1. Body and viscous forces are neglected,
2. No heat addition to fluid,
3. The only work is flow work,
4. Fluid obeys the ideal gas equation of state (restricts equation (3-5) only), and
5. Flow is axi-symmetric and compressible.

The five equations must be solved simultaneously in order to obtain the five unknowns p, ρ, v, u and e. As of this date, there are no analytical methods available by which a complete and exact solution may be obtained. Even the classical methods of finite difference analyses will not provide a solution when the flow field involved contains local steep gradients or discontinuities of the dependent variables. For this reason, much attention has been given to the development of new numerical techniques which will handle strong gradients or shocks. One such development has been the evolution of a technique which uses an artificial dissipative term. The basis of this concept was provided by von Neumann and Richtmyer (2), in 1950. Since that time, a number of authors have investigated numerical solutions of this type (3), (25), (26). A history of the development of these methods is given in Chapter II, reference (4), Tyler.

The particular method used in this study was originated by Rusanov (3); the detailed derivation of Rusanov's work has been given by

Tyler (4). The principal feature of this method is that by adding second order blurring terms to the original flow equations, the discontinuities present in the flow field can be made to diffuse over a finite distance. By diffusing the strong gradients, the classical difference techniques are adequate to obtain approximate solutions of the partial differential equations throughout the entire flow field. Since the terms added are based on curvature, their magnitude is appreciable only near large changes in slope.

The characteristics which the additional terms must possess are specified by von Neumann and Richtmyer (2) in their original paper:

1. The general flow equations with the addition of the "blurring" terms must possess solutions without discontinuities;
2. The thickness of shocks present must be of the same order as the distance between grid mesh points (Δx);
3. The effect of the "blurring" terms must be negligible outside the shock regions;
4. The Rankine-Hugoniot equations must hold across the shocks.

Blurring Terms

The general form of the flow equation with the additional blurring terms for two-dimensional rectangular coordinates (x,y) is:

$$\frac{\partial f}{\partial t} + \frac{\partial F^x}{\partial x} + \frac{\partial F^y}{\partial y} = \frac{\partial}{\partial x}\left(A(x,y,t)\frac{\partial f}{\partial x}\right) + \frac{\partial}{\partial y}\left(B(x,y,t)\frac{\partial f}{\partial y}\right), \qquad (3\text{-}7)$$

where A(x,y,t) and B(x,y,t) are the blurring coefficients which are evaluated by applying the Fourier stability technique to the above differential equation (References 3 and 4). The transformation of equation (3-7) from rectangular coordinates (x,y) to axi-symmetric coordinates (r,z) gives an added ψ term on the left hand side. Also, all x-coordinates are replaced by z-coordinates and all y-coordinates are replaced by r-coordinates. Appendix A presents the transformation of the blurring terms [the right hand side of equation (3-7)]. The final form of the transformed equation is

$$\frac{\partial f}{\partial t} + \frac{\partial F^z}{\partial z} + \frac{\partial F^r}{\partial r} + \psi = \frac{1}{r}\frac{\partial}{\partial r}\left(rB(r,z,t)\frac{\partial f}{\partial r}\right) + \frac{\partial}{\partial z}\left(A(r,z,t)\frac{\partial f}{\partial z}\right). \quad (3\text{-}8)$$

Numerical Difference Scheme

Rusanov's technique requires that the field of interest be divided into a mesh point system. Figure 3 indicates how the cone-cylinder configuration fits into the mesh point system. The cone surface coincides with the diagonal of the mesh point array and the cylinder surface lies on a row of mesh points. Figure 4 shows the details of the mesh net used. The increment of the independent variables (r,z,t) is denoted in the differencing scheme as (h_2, h_1, τ). A point is located in the mesh by $(r,z,t) = (\ell h_2, m h_1, n\tau)$.

The derivatives of equation (3-8) will be approximated by using a truncated Taylor series. Centered differences will be applied to spatial derivatives for points lying interior to the boundaries, and derivatives with respect to time approximated with forward differences. A discussion of the specific boundary conditions is given in Chapter IV.

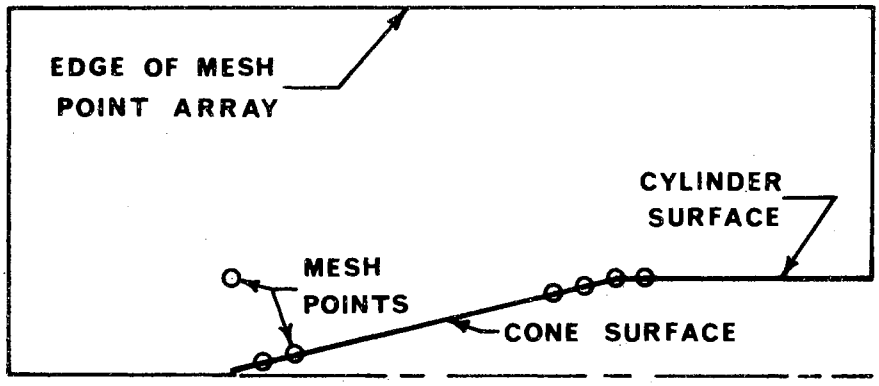

Figure 3. Cone-Cylinder Configuration Showing Some Typical Mesh Points

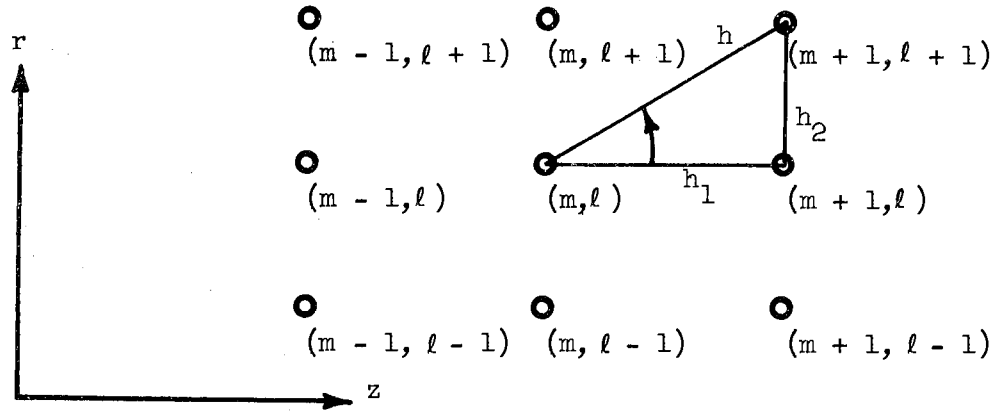

Figure 4. Finite Difference Net Notation

Equation (3-8) can now be approximated for field points (points lying within the mesh point boundaries) by using the above information and the mesh net notation as:

$$\frac{f^{n+1}_{m,\ell} - f^{n}_{m,\ell}}{\tau} + \left(\frac{F^{z}_{m+1,\ell} - F^{z}_{m-1,\ell}}{2h_1}\right)^n + \left(\frac{F^{r}_{m,\ell+1} - F^{r}_{m,\ell-1}}{2h_2}\right)^n + \psi^{n}_{m,\ell}$$

$$= \frac{1}{h_1^2}\left(A^{n}_{m+\frac{1}{2},\ell}(f_{m+1,\ell} - f_{m,\ell})^n - A^{n}_{m-\frac{1}{2},\ell}(f_{m,\ell} - f_{m-1,\ell})^n\right) \qquad (3\text{-}9)$$

$$+ \frac{1}{(\ell-1)h_2^2}\left((\ell-\tfrac{1}{2})B^{n}_{m,\ell+\frac{1}{2}}(f_{m,\ell+1} - f_{m,\ell})^n - (\ell-\tfrac{3}{2})B^{n}_{m,\ell-\frac{1}{2}}(f_{m,\ell} - f_{m,\ell-1})^n\right).$$

The following symbols are defined:

$$A^{n}_{m,\ell} = \frac{h_1^2}{2}\alpha^{n}_{m,\ell}, \qquad (3\text{-}10)$$

$$B^{n}_{m,\ell} = \frac{h_2^2}{2}\beta^{n}_{m,\ell}, \qquad (3\text{-}11)$$

and

$$A_{m+\frac{1}{2},\ell} = \tfrac{1}{2}(A_{m+1,\ell} + A_{m,\ell}),\ B_{m,\ell+\frac{1}{2}} = \tfrac{1}{2}(B_{m,\ell+1} + B_{m,\ell}), \qquad (3\text{-}12)$$

$$K_1 = \frac{\tau}{h_1}, \qquad (3\text{-}13)$$

$$K_2 = \frac{\tau}{h_2}, \qquad (3\text{-}14)$$

$$K = (K_1^2 + K_2^2)^{\frac{1}{2}}, \qquad (3\text{-}15)$$

$$K_1 = K\sin(\chi) \text{ and } K_2 = K\cos(\chi). \qquad (3\text{-}16)$$

Upon substituting equations (3-9) through (3-15) into equation (3-8) and solving for $f^{n+1}_{m,\ell}$, the following is obtained:

$$f^{n+1}_{m,\ell} = f^{n}_{m,\ell} - \frac{K_1}{2}(F^{z}_{m+1,\ell} - F^{z}_{m-1,\ell})^{n} - \frac{K_2}{2}(F^{r}_{m,\ell+1} - F^{r}_{m,\ell-1})^{n} - \tau\psi^{n}_{m,\ell}$$

$$+ \frac{1}{4}\Bigg((\alpha^{n}_{m+1,\ell}(f_{m+1,\ell} - f_{m,\ell})^{n} + \alpha^{n}_{m-1,\ell}(f_{m-1,\ell} - f_{m,\ell})^{n}$$

$$+ \alpha^{n}_{m,\ell}(f_{m+1,\ell} + f_{m-1,\ell} - 2f_{m,\ell})^{n}$$

$$+ \frac{(\ell-\frac{1}{2})}{(\ell-1)}(\beta^{n}_{m,\ell+1} + \beta^{n}_{m,\ell})(f_{m,\ell+1} - f_{m,\ell})^{n}$$

$$- \frac{(\ell-\frac{3}{2})}{(\ell-1)}(\beta^{n}_{m,\ell-1} + \beta^{n}_{m,\ell})(f_{m,\ell} - f_{m,\ell-1})^{n}\Bigg) . \qquad (3\text{-}17)$$

The stability criteria given by Rusanov (3) specify

$$\alpha^{n}_{m,\ell} = \alpha K(w+c)^{n}_{m,\ell} \sin^2(\chi),$$

$$\beta^{n}_{m,\ell} = \alpha K(w+c)^{n}_{m,\ell} \cos^2(\chi),$$

and

$$\sigma_o^2 \leq \sigma_o \omega \leq 1,$$

where σ_o is the maximum value of σ in the flow field at time n. The equations for α and β relate the amount of artificial dissipation and the time increment. The value of σ_o in conjunction with $(w+c)_{max}$ determines the time increment between any two successive time steps. From the stability criteria $\sigma^{n}_{m,\ell} = K(w+c)^{n}_{m,\ell}$, then $\sigma^{n}_{o} = K(w+c)^{n}_{max}$. The summation of time ellapsed is then given by

$$\Sigma K = \Sigma \frac{\sigma^{n}_{o}}{(w+c)^{n}_{max}} . \qquad (3\text{-}18)$$

A detailed presentation may be found in Walker (6).

Equation (3-17) can be used only to determine properties at field points; other techniques must be applied at the boundaries to approximate

local first and second partials. At the upper boundary the first partial in the r-direction at (m,ℓ) was approximated by a backward difference using properties at (m,ℓ) and $(m,\ell-1)$. The second partial in the r-direction was approximated by using properties at (m,ℓ), $(m,\ell-1)$, and $(m,\ell-2)$. At the right hand boundary, points (m,ℓ) and $(m-1,\ell)$ were used to obtain first partials in the z-direction, while the second derivative in this direction was obtained by using (m,ℓ), $(m-1,\ell)$, and $(m-2,\ell)$. At the axis of symmetry and the cylinder surface, all first partials were forced to zero by using the reflective principle. This technique required the properties one row of mesh points below the line of symmetry to be given values identical to the properties one row above the line of symmetry, except for the value of r-velocity which was given identical magnitude and opposite direction. The cone surface was treated as if it were a two-dimensional wedge, as in Rusanov's investigations (3). Details of this approximation and other attempted methods are given in Chapter IV. Although other methods were investigated at all boundaries, the ones presented above proved to be the most satisfactory.

During the real gas study, all of the above equations and ideas were used with the exception of equation (3-5). The development of this equation required the assumption of an ideal gas. In order to avoid ideal gas concepts, a relationship other than equation (3-5) was used to relate pressure to the other flow properties for the real gas case. This was accomplished by using a "semi-physical fit" to the equation of state of air,

$$p = (\gamma-1)\rho\epsilon. \qquad (3\text{-}19)$$

Doan and Nickel (27) curve-fit tabulated data provided by the National

Bureau of Standards; the maximum error of the resulting curve is five per cent. The quantity $(\gamma-1)$ can be found knowing density and internal energy, which is computed from the continuity and energy equations. Using these quantities, pressure can be found directly from equation (3-19).

Presented below is the final form of Doan's equations:

$$\gamma-1 = \left\{0.161 + 0.255\, e^{-\epsilon/4.46} f_1 + 0.280\, e^{-\epsilon/6.63}(1-f_1) + 0.137\, e^{-\epsilon/25.5} f_2 + 0.050\, f_3\right\}\left(\frac{\rho}{\rho_o}\right)^{\alpha(\epsilon)},$$

where

$$\alpha(\epsilon) = 0.048\, f_1 \log_{10}\epsilon + 0.032(1-f_1)(1-f_2)\log_{10}\epsilon + 0.045\, f_2,$$

$$f_1 = \left[\exp\left(\frac{\epsilon-\epsilon_1}{\Delta\epsilon_1}\right) + 1\right]^{-1} \qquad f_2 = \left[\exp\left(\frac{\epsilon_2-\epsilon}{\Delta\epsilon_2}\right) + 1\right]^{-1}$$

$$f_3 = \left[\exp\left(\frac{\epsilon_3-\epsilon}{\Delta\epsilon_3}\right)\right]^{-1} \qquad \epsilon_1 = 8.5 + 0.357 \log_{10}\left(\frac{\rho}{\rho_o}\right),$$

$$\epsilon_2 = 45.0\left(\frac{\rho}{\rho_o}\right)^{0.0157}, \qquad \Delta\epsilon_1 = 0.975\left(\frac{\rho}{\rho_o}\right)^{0.05},$$

$$\Delta\epsilon_2 = 4.0\left(\frac{\rho}{\rho_o}\right)^{0.085}, \qquad \epsilon_3 = 160.0 \text{ and } \Delta\epsilon_3 = 6.0\,.$$

Non-Dimensionalizing Dependent Variables

In order to simplify the numerical calculations the terms of the flow equations are made dimensionless by applying the following procedure: pressures are divided by p_1, densities by ρ_1, and velocities by p_1/ρ_1.

The energy term becomes, in turn, dimensionless with respect to p_1.

The properties in region "1" were selected to be the ones which initially surround the cone-cylinder in Phase 1. Therefore, the final data obtained in all three phases can be returned to their dimensional form by multiplying each property by its respective non-dimensionalizing quantity.

The dimensional values in the Phase 2 free stream of the real gas case are standard atmospheric conditions at an altitude of 40,000 feet. They are made dimensionless in such a way that the free stream dimensionless pressure and density are identical to the corresponding pressure and density in the ideal gas case. These values were selected to make it convenient to compare the two theories.

CHAPTER IV

BOUNDARY STUDY

The method by which the boundary mesh points are treated greatly influences the solution throughout the mesh point array. For this reason a considerable amount of time was spent investigating each of the seven boundaries included in the cone-cylinder problem, in order to obtain a viable solution. These boundaries, indicated by number in Figure 5, are:

1. axis of symmetry,
2. stagnation point,
3. cone surface,
4. cone-cylinder intersection,
5. cylinder surface,
6. right hand boundary, and
7. upper boundary.

The property values at the upstream left boundary are specified and therefore no special numerical technique is required. The method used to evaluate the flow properties at each boundary will be discussed separately, except where coupling between two boundaries were observed.

Axis of Symmetry

The axis of symmetry (r=0) was treated by applying the reflection

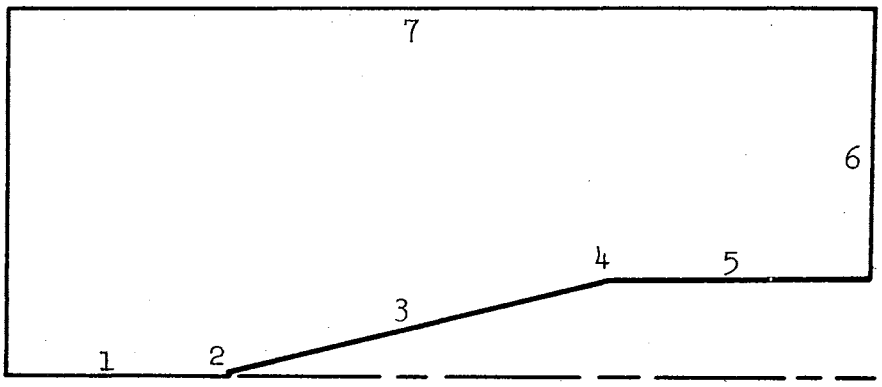

Figure 5. Seven Boundary Locations

principle, as discussed in Chapter III. The principle is valid at this boundary because the boundary is, in fact, an axis of symmetry. One difficulty which does occur at the axis is the evaluation of the term (v/r). At r=0 (ℓ=1), this term is undefined, because v is also zero. The approximation made is

$$\left(\frac{v}{r}\right)_{\ell=1} \cong \left(\frac{v}{r}\right)_{\ell=2}.$$

Stagnation Point

The stagnation point is extremely difficult to handle by numerical methods because it is mathematically a branch point. Although most analytical methods avoid the point, satisfactory results were obtained by the following numerical procedure. When the property values at the stagnation point were obtained by linear extrapolation using surrounding mesh points, the resulting stagnation pressure and density were always too low. Treating the point like a wall perpendicular to the free stream flow also gave stagnation properties that were too low. The best results at the stagnation point were obtained by isentropically stagnating the properties at one mesh point upstream. From isentropic relations:

$$\rho(\text{stagnation}) = \rho_{m-1,\ell}\left(1 + \frac{\gamma-1}{2} M^2\right)^{\frac{1}{\gamma-1}} \text{ and}$$

$$p(\text{stagnation}) = p_{m-1,\ell}\left(1 + \frac{\gamma-1}{2} M^2\right)^{\frac{\gamma}{\gamma-1}},$$

where M is the Mach number at (m-1,1).

This approximation works well for cases in which the bow shock is detached far enough from the cone nose so that the first mesh point in

front of the nose is downstream from the shock. Because higher Mach numbers force the bow wave to stand closer to the cone nose, this treatment was more effective for Phase 1 calculations than for Phase 2 or Phase 3.

Cone Surface

Two different coordinate systems and two methods of extrapolation were tried on the cone surface; each of the methods had advantages and disadvantages. The one ultimately selected for use was chosen because it produced reasonable results and was not too cumbersome numerically. In the first method the flow equations were derived in the spherical coordinate system. All partials with respect to Φ were then set equal to zero (see Figure 6). This coordinate system was applied only to points lying on the cone surface; it was not used throughout the flow field. Instability always occurred at the first mesh point downstream from the cone nose when the spherical coordinate system was used. A study was made using a 30 degree half-angle-wedge to investigate the possibility of extrapolating toward the surface to evaluate the four flow properties at this boundary. One case consisted of using the average linear extrapolations in the r- and z- directions toward the surface. This resulted in steady-state surface pressures that were approximately 70% too high. Further, when extrapolation was carried out only in the r-direction, the surface pressures were approximately 30% too low. But when the extrapolation in the r-direction was used only to obtain the pressure, density, and z-mass flux, and the r-mass flux was obtained by requiring that the total velocity vector be in the direction of the body

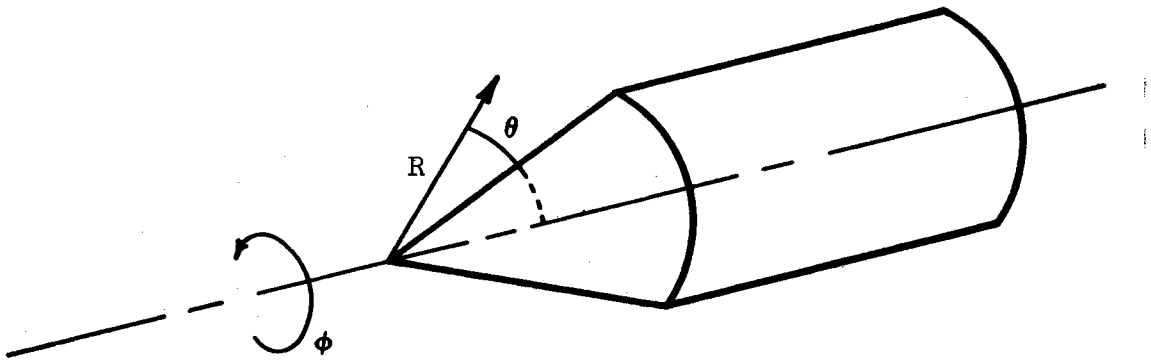

Figure 6. R,Φ,θ Coordinate System Used on the Cone Surface

surface, the error in the surface pressures dropped to approximately 10%. However, the pressures were 40% too low, when the same extrapolation procedure was applied to a 13.347 degree half-angle-cone. Thus, the accuracy of the method varied with body configuration and apex angle. The undesirable effect of all the extrapolation procedures for wedge and cone configurations was that it caused the pressure at (I,2) to be too low (where I is the z-coordinate location of the nose), consequently distorting the front of the bow wave.

The second coordinate system investigated, and the one ultimately used, was a two-dimensional rotation of the axis about a mesh point on the cone surface. The cone surface was treated, in accordance with Rusanov's methods, as if it were locally two-dimensional. This two-dimensional treatment was an approximation. The flow equations, in rectangular coordinates, were rotated through the angle χ, and these transformed equations replaced by difference equations. Thus, the coordinates of calculation were along and perpendicular to the body surface. There was no need to calculate the r-momentum equation in the rotated coordinate system because r-momentum was identically zero. The artificial viscosity terms perpendicular to the wall were set equal to zero. This required that shocks intersecting the body be perpendicular to it at the point of intersection.

The mesh points used for numerical calculations at (m,ℓ) were (m,ℓ), $(m+1,\ell+1)$, $(m-1,\ell-1)$ and $(*)$ (see Figure 7). Properties at $(*)$ were obtained by linear interpolation between $(m,\ell+1)$ and $(m-1,\ell)$. The location * is at a point lying perpendicular to the surface from mesh point (m,ℓ). Partials perpendicular to the surface were approximated

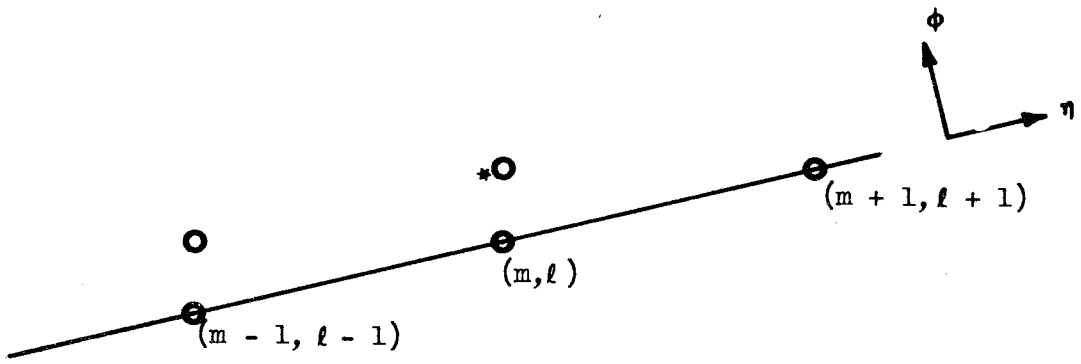

Figure 7. Mesh Points Along the Cone Boundary

by an off-centered difference, which was found by using properties at (*) and (m,ℓ). The partials along the wall were calculated using mesh points $(m+1,\ell+1)$, (m,ℓ) and $(m-1,\ell-1)$. The final form of the equation is:

$$\tilde{f}^{n+1}_{m,\ell} = \tilde{f}^{n}_{m,\ell} - \tau\tilde{\psi}_{m,\ell} - \frac{K_1 \cos(\chi)}{2}\left(\tilde{F}^{\eta}_{m+1,\ell+1} - \tilde{F}^{\eta}_{m-1,\ell-1}\right)^n$$
$$- K\left(\cos^2(\chi)\tilde{F}^{\Phi}_{m,\ell+1} + \sin^2(\chi)\tilde{F}^{\Phi}_{m-1,\ell}\right)^n$$
$$+ \frac{\cos^2(\chi)}{2}\left(\frac{\tilde{\tilde{\alpha}}_{m+1,\ell+1} + \tilde{\alpha}_{m,\ell}}{2}\left(\tilde{f}_{m+1,\ell+1} - \tilde{f}_{m,\ell}\right)\right.$$
$$\left. + \frac{\tilde{\alpha}_{m-1,\ell-1} + \tilde{\alpha}_{m,\ell}}{2}\left(\tilde{f}_{m-1,\ell-1} - \tilde{f}_{m,\ell}\right)\right)^n.$$

All quantities with the sign $(\sim)$ were computed by the same formula as the corresponding quantities in equation (3-17) without this sign, but u and v are replaced by $\tilde{u}$ and $\tilde{v}$, where:

$$\tilde{u} = u\cos(\chi) + v\sin(\chi), \text{ and}$$

$$\tilde{v} = -u\sin(\chi) + v\cos(\chi).$$

It is noted that, on the cone surface

$$\rho_{m,\ell} = \tilde{\rho}_{m,\ell}$$

$$(\rho u)_{m,\ell} = (\rho\tilde{u})_{m,\ell}\cos(\chi),$$

$$(\rho v)_{m,\ell} = (\rho\tilde{u})_{m,\ell}\sin(\chi),$$

$$e_{m,\ell} = \tilde{e}_{m,\ell} \text{ and}$$

$$p_{m,\ell} = \tilde{p}_{m,\ell}.$$

With the rotated coordinates, as with the (r,θ) coordinates, the calculations at the first mesh point back of the cone nose had a tendency to become unstable. In an attempt to eliminate the instability behind the nose, the artificial viscosity term at this location was increased

by a factor of two. This increase helped the local property values but they were still unreasonable.

On large angle cones (30 degrees), calculations at the first mesh point behind the cone nose were satisfactory, while on small angle cones (13.347 degrees), the instability mentioned above always occurred. To investigate the possibility that this instability problem might be connected with the relative mesh rectangle dimensions, a different cone mesh combination was investigated. A mesh point system was devised in which the cone did not pass through the diagonal of the mesh point array but, instead, was constructed according to Figure 8. As the figure indicates, a more nearly square mesh point array could be used for a small angle cone.

The mesh points lying on the cone surface were treated in the same manner as the surface mesh points in the previously discussed two-dimensional rotation system. The properties, for the (n+1) time plane at mesh points geometrically similar to point C (Figure 8, points lying a distance $\frac{1}{2}h_2$ from the cone surface), were calculated using n^{th} time plane properties at points B, C, D, E, and F. Since point B is not a regular mesh point, properties at this location were calculated by using a linear interpolation between points A and C. Similarly, for the properties at D, a linear interpolation between F and G was employed. With these values, point C was treated as a regular field point, making the necessary adjustment for the decreased distance between points in the r-direction. The new mesh system did not relieve the problem of instability behind the cone nose; the calculations at point G became unstable.

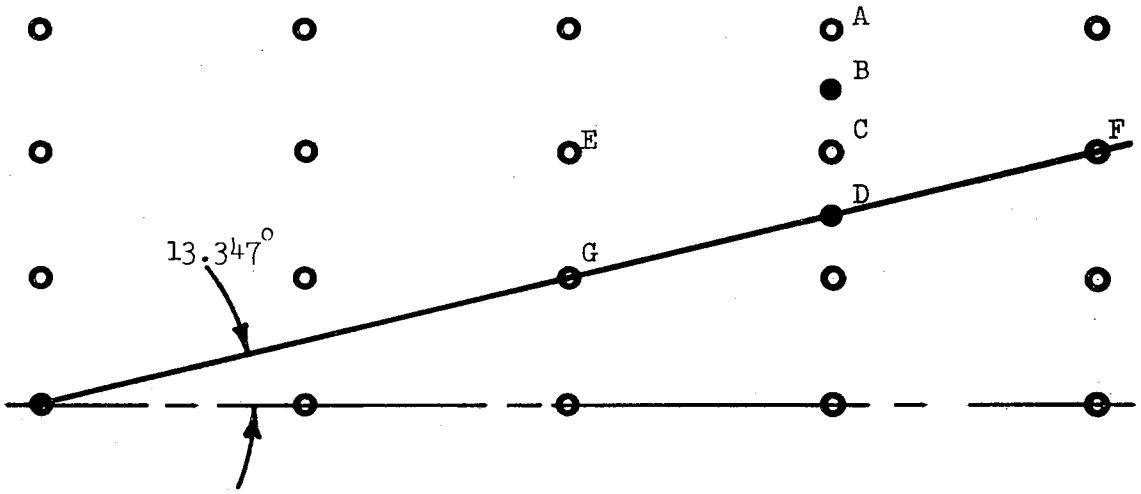

Figure 8. Alternate Mesh Net Configuration

The first mesh point behind the cone nose is located in a region containing high expansion gradients. The flow goes from zero velocity at the stagnation point to a supersonic state at a short distance downstream. The applied numerical schemes were not adequate to handle this phenomenon. Therefore, to avoid expanding the flow along the cone from zero velocity to high speed flow, the body shape was changed slightly in the nose region (see Figure 9). This new configuration will be discussed in detail, because it was the configuration ultimately used. The cone was blunted by moving the stagnation point downstream one mesh point to location F (see Figure 9). The properties at point F were then calculated by isentropically stagnating the properties at C. Point C was treated in the same manner as the other points lying on the axis of symmetry. Point D was considered to be on the cone surface; therefore, points A, B, C, D, and E from time plane n were used to calculate the properties at D for time plane (n+1). As a result of using the blunted cone configuration, the calculations at point D do not involve a mesh point with zero velocity and mesh points with large velocities. For cones with small apex angles, flow properties calculated by this method were superior to those obtained by any other method.

Cone-Cylinder Intersection

The mesh point lying on the cone-cylinder intersection was treated by two methods. In the first, the point was assumed to be on the cylinder and was considered the same as other cylinder points. The three nearest mesh points were used for the calculations. In the second method, the mesh point was considered to be on the cone surface. The

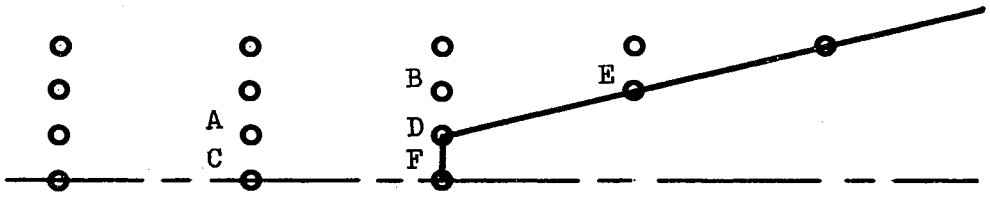

Figure 9. Blunt Nose Cone Configuration

scheme used at other cone mesh points was employed at the cone-cylinder mesh point. Flow property values obtained by the first procedure were similar to those obtained at the other cylinder points, and the second procedure gave property values similar to those at other neighboring cone mesh points. The results of both methods were reasonably realistic, so the mesh point was considered as a cone surface point for all production runs.

Cylinder Surface

The method which was used on the cylinder surface was suggested by Rusanov (3). This treated the point as though it lay on a surface of symmetry. As this procedure gives reasonable results and the cylinder is downstream from the region of primary interest, no other boundary condition was investigated.

Upper Boundary

When a strong shock extends through the upper boundary the numerical technique at this location becomes critical. An infinite cone configuration, i.e., a cone which extends to the right boundary, was used to investigate this region to amplify the difficulty. Because the shock was not weakened by the termination of the cone, the shock wave extended through the upper boundary. Three methods were used to study the problem.

First, a second order extrapolation was applied at this boundary using

$$f^{n+1}_{m,\ell_{max}} = 3f^{n+1}_{m,\ell_{max}-1} - 3f^{n+1}_{m,\ell_{max}-2} + f^{n+1}_{m,\ell_{max}-3}.$$

Instability, which originated in the region where the shock extended through the upper boundary, resulted. The instability in this region quickly spread to other parts of the flow field. Although this second order extrapolation had been used by other authors, they did not use it on boundaries through which a strong shock passed. Second, a linear extrapolation toward the upper boundary was accomplished by using

$$f^{n+1}_{m,\ell_{max}} = 2f^{n+1}_{m,\ell_{max}-1} - f^{n+1}_{m,\ell_{max}-2}.$$

The calculations at the upper boundary remained stable and the results were reasonable.

The third method applied the differenced form of the partial differential equations. All first partials in the r-direction were based upon points (m,ℓ) and $(m,\ell-1)$. These partial derivatives were uncentered; consequently the accuracy was one lower order than partials approximated by central differences. The second derivatives were based upon points (m,ℓ), $(m,\ell-1)$, and $(m,\ell-2)$. This approximation held the curvature at (m,ℓ) and $(m,\ell-1)$ equal for time plane n. The difference equation based upon these premises is:

$$\begin{aligned} f^{n+1}_{m,\ell} = f^{n}_{m,\ell} - \tau\psi^{n}_{m,\ell} - \frac{K_1}{2}(F^{z}_{m+1,\ell} - F^{z}_{m-1,\ell})^{n} - K_2(F^{r}_{m,\ell} - F^{r}_{m,\ell-1})^{n} \\ + \frac{1}{4}\Big(\alpha_{m+1,\ell}(f_{m+1,\ell} - f_{m,\ell}) + \alpha_{m-1,\ell}(f_{m-1,\ell} - f_{m,\ell}) \\ + \alpha_{m,\ell}(f_{m+1,\ell} + f_{m-1,\ell} - 2f_{m,\ell}) + \beta_{m,\ell}(f_{m,\ell} - f_{m,\ell-1}) \\ + \beta_{m,\ell-2}(f_{m,\ell-2} - f_{m,\ell-1}) + \beta_{m,\ell-1}(f_{m,\ell} + f_{m,\ell-2} - 2f_{m,\ell-1})\Big)^{n}. \end{aligned} \tag{3-19}$$

This method of calculation was the most consistent with the field point method and provided realistic results.

Right Boundary

The treatment of the right boundary was not as critical as the treatment of the upper boundary since the flow upstream was supersonic. Two different methods worked equally well and a third caused instability. The first, which was ultimately used, employed the same technique on the right boundary as was used on the upper boundary. The first partials in the z-direction were calculated using points (m,ℓ) and $(m-1,\ell)$; the second partials were based upon points (m,ℓ), $(m-1,\ell)$, and $(m-2,\ell)$. These approximations resulted in

$$f^{n+1}_{m,\ell} = f^{n}_{m,\ell} - \tau\psi^{n}_{m,\ell} - K_1\left(F^{z}_{m,\ell} - F^{z}_{m-1,\ell}\right)^{n} - \frac{K_2}{2}\left(F^{r}_{m,\ell+1} - F^{r}_{m,\ell-1}\right)^{n}$$

$$+ \frac{1}{4}\Big(\alpha_{m,\ell}\left(f_{m,\ell} - f_{m-1,\ell}\right) + \alpha_{m-2,\ell}\left(f_{m-2,\ell} - f_{m-1,\ell}\right)$$

$$+ \alpha_{m-1,\ell}\left(f_{m,\ell} + f_{m-2,\ell} - 2f_{m-1,\ell}\right) + \beta_{m,\ell+1}\left(f_{m,\ell+1} - f_{m,\ell}\right)$$

$$+ \beta_{m,\ell-1}\left(f_{m,\ell-1} - f_{m,\ell}\right) + \beta_{m,\ell}\left(f_{m,\ell+1} + f_{m,\ell-1} - 2f_{m,\ell}\right)\Big)^{n}. \quad (3\text{-}20)$$

The second successful method shifted the properties from the (N-1) column to the Nth column during each time plane. This means that at every time plane the slope at the right boundary equaled zero, or:

$$f^{n}_{(N-1,\ell)} = f^{n}_{(N,\ell)}.$$

A third method, linear extrapolation along a row toward the N^{th} column, gave unstable results. The instability started during the period of time when the shock passed through the boundary. Figure 10 indicates how the linear extrapolation, when applied at the moment the shock passed out of the field, resulted in negative values of pressures, which caused instability. The negative slope taken from the first two mesh

points to the left of the right mesh boundary was so large that it yielded a negative pressure at that boundary.

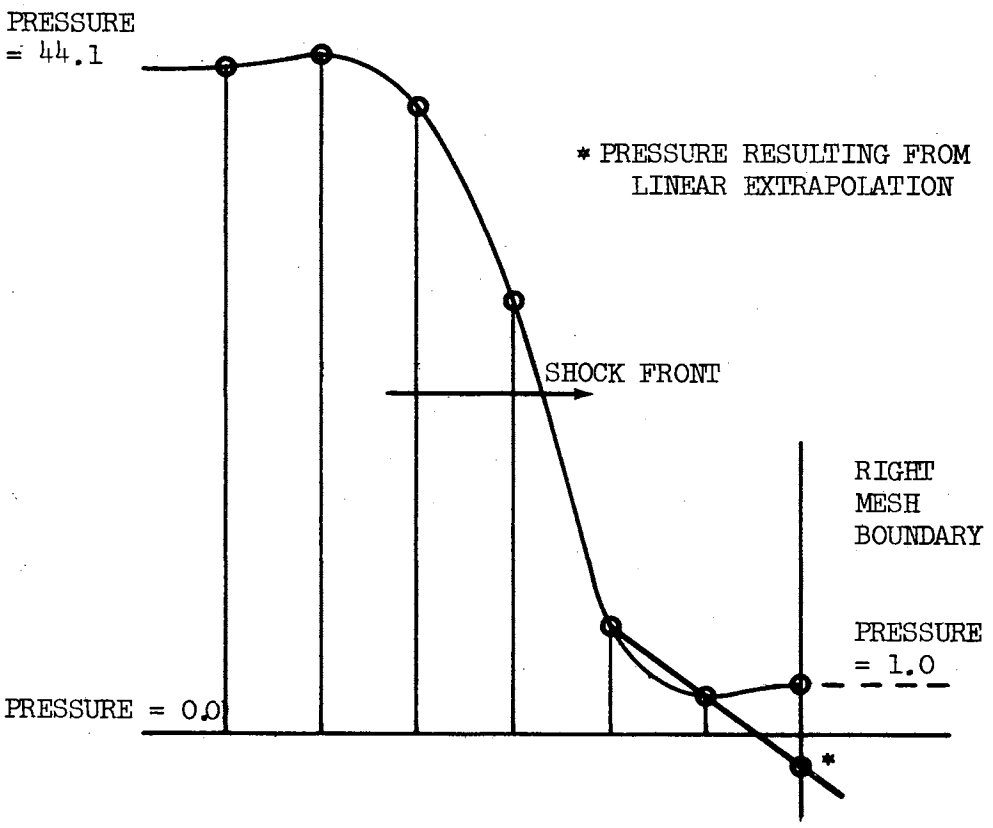

Figure 10. Shock Front as It Moves Through the Right Boundary

CHAPTER V

APPLICATION OF NUMERICAL TECHNIQUE TO THE EXITING AND ENTERING PROBLEM

The numerical technique presented in Chapter III, together with the boundary conditions discussed in Chapter IV, were applied to the cone-cylinder configuration for the three different Phases. The initial data for the ideal gas, were obtained with the aid of the ideal gas tables, reference 28. The real gas tables, reference 29, were used for the real gas case.

Phase 1 consisted of allowing a normal shock to propagate over the cone-cylinder, which was initially surrounded by air at zero velocity. The same flow could be obtained experimentally by testing a cone-cylinder model in a single diaphragm air/air shock tube, with the initial pressure ratio across the diaphragm approaching infinity. After the shock propagated over the body, a steady-state, low supersonic flow existed, such as the state which could exist about a cone-cylinder within a blast sphere immediately prior to exiting through the blast front. Initial data for this phase are listed in Tables I and II under regions 1 and 2.

A normal shock was introduced at the left boundary of the mesh point array during the initial time plane of Phase 2. The initial data for this phase were that of the final time plane of Phase 1, in addition

TABLE I

INITIAL FLOW DATA FOR IDEAL GAS

Region[1]	Density	z-Mass Flux	r-Mass Flux	Pressure
1	1.0	0.0	0.0	1.0
2	5.301	31.23	0.0	44.1
3	1.140	12.83	0.0	2.205

TABLE II

INITIAL FLOW DATA FOR REAL GAS

Region[1]	Density	z-Mass Flux	r-Mass Flux	Pressure	Specific Heat Ratio
1	1.0	0.0	0.0	1.0	1.405
2	5.52	32.11	0.0	44.1	1.375
3	1.140	12.78	0.0	2.205	1.405
4	5.52	91.5	0.0	44.1	1.375

[1]The regions are defined as follows:

1 Downstream from the normal shock which initially exits in Phase 1
2 Left boundary of the mesh point array during Phase 1
3 Left boundary of the mesh point array during Phase 2
4 Left boundary of the mesh point array during Phase 3

to the data listed for region 3 in Tables I and II. The data given for region 3 were overlayed in the first column of mesh points. The normal shock which was inserted in this manner propagated toward the right boundary. This simulated exiting of the cone-cylinder from the high pressure, low relative velocity region inside the blast sphere, into the low pressure, high relative velocity region outside the blast sphere. The duration of Phase 2 was continued until a new steady-state bow wave was established over the cone-cylinder, representing the projectile moving through the undisturbed atmosphere at a relatively high Mach number. This sequence of events is demonstrated by Figure 2.

It was found after calculating Phases 1 and 2 that the difference in the results between the ideal and real gas case was insignificant. Therefore, only the real gas problem was computed for Phase 3. The initial data for Phase 3 consisted of inserting a normal shock at the left boundary of the last time plane of Phase 2. The properties to the left of the shock are listed under region 4, Table II. As the normal shock propagated from left to right, it interacted with the initial steady-state bow wave of Phase 3. The transient flow of Phase 3 simulated the passing of the body from a high velocity, low pressure region outside the blast front into a region of higher relative velocity and pressure. This second region corresponds to the location immediately inside a large radius blast sphere (see Figure 1c).

All production was done on the Oklahoma State University IBM 7040 digital computer. Twenty-eight mesh points in the z-direction and forty-nine points in the r-direction were used for the ideal gas program. The real gas problem was programmed with 28 by 45 mesh points

in the z- and r-directions, respectively. Fewer mesh points were used for the real gas problem, because additional storage was required to store an array of specific heat ratios. The machine time required for the ideal gas program was approximately four-tenths of a minute per time plane; the real gas program took slightly longer. The flow diagram for the computer program is listed in Appendix C.

The half apex angle of the cone was 13.347 degrees. The cone nose was located at m = 8; the cone-cylinder intersection at m = 20; and the ratio of specific heats for the ideal gas was set equal to 1.4. The magnitude of the artificial damping coefficient (ϖ) was 1.5, and the time increment $\sigma_o = 0.5$.

Phase One Results

The main purpose of running Phase 1 (Figure 12) was to obtain a steady-state bow wave which could be used as initial data for Phase 2. There are, however, some aspects of the transient state worth noting. The sonic circle, predicted in an analytical study by Smyrl (10) and observed by Klein (24) in a water table analogy, was not observable in the small angle cone case. However, when the same shock front was passed over an infinite cone with a half apex angle of thirty degrees, the sonic circle was present, as can be seen in Figure 11.

The cone-cylinder configuration was calculated for both real and ideal gas. In each case a steady state was obtained in which the maximum pressure change for one time plane was less than 0.13%. The steady-state condition can be seen by comparing Figure 12, Parts "e" and "f". They show that the shape of the steady-state shock pattern

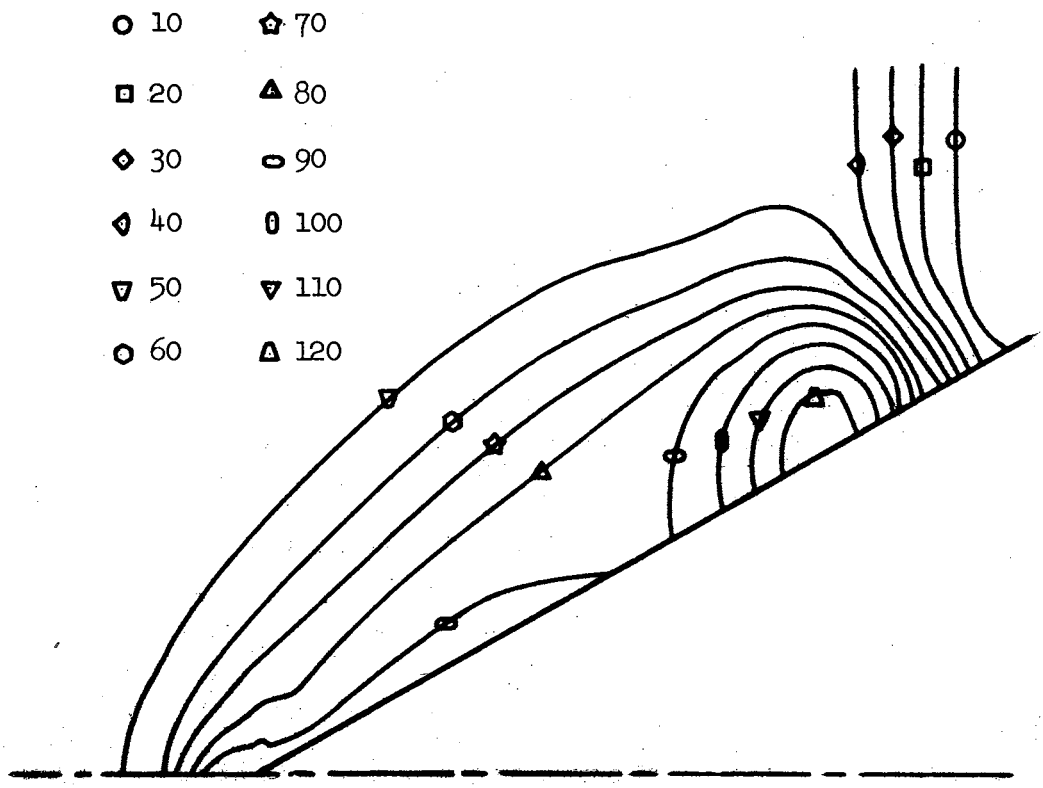

Figure 11. Thirty Degree Cone Showing Sonic Circle Using Isobars

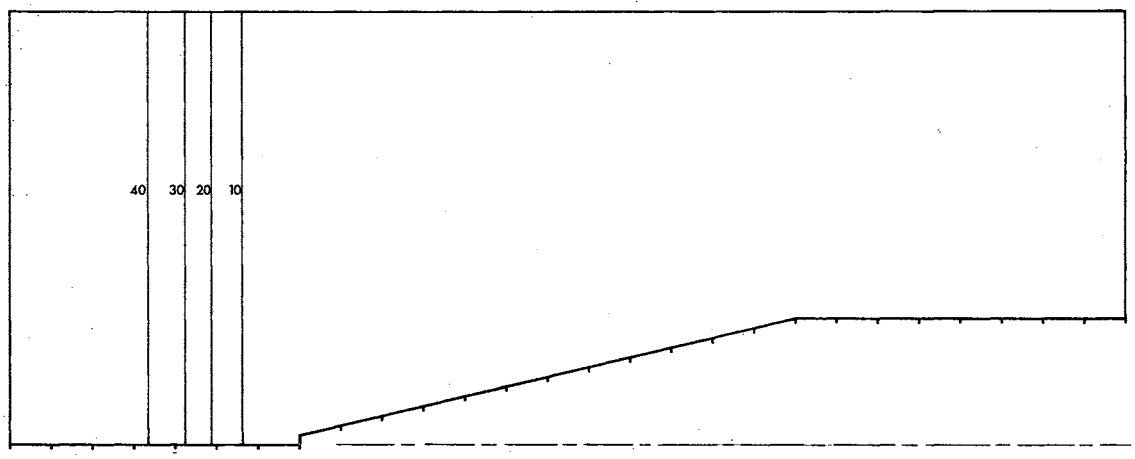

(a) TP=50 (ΣK=2.702)

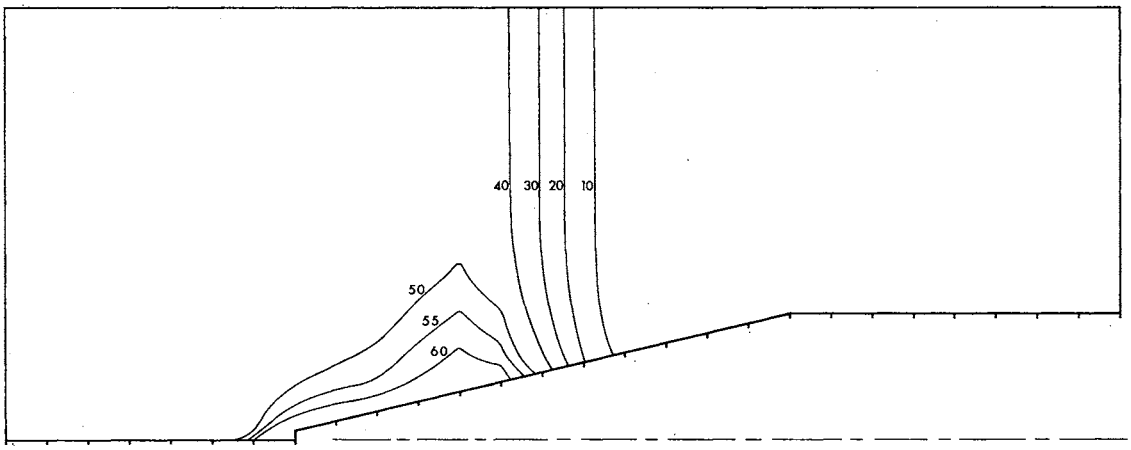

(b) TP=150 (ΣK=7.983)

Figure 12. Constant Pressure Lines for Phase I: Normal Shock Passing Over Stationary Body (Initial Conditions are given in Table II)

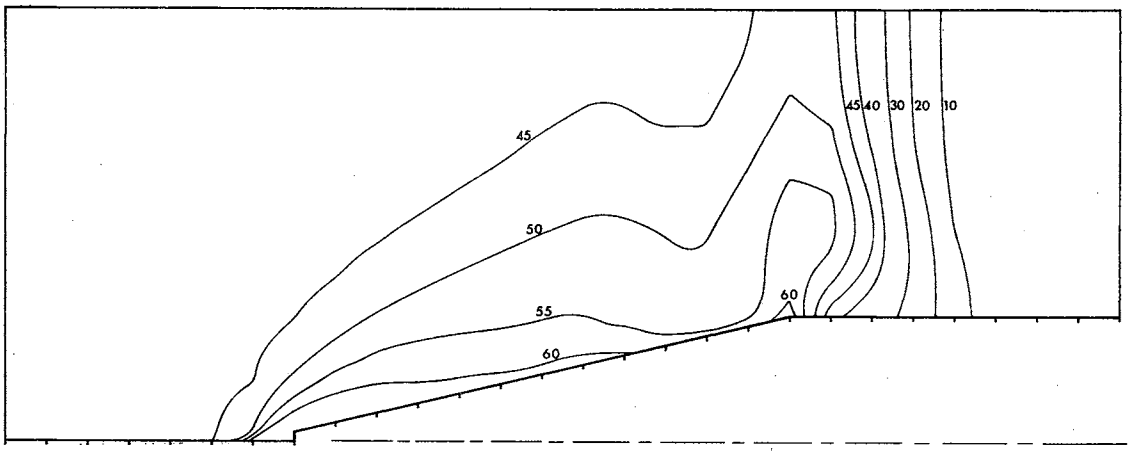

(c) TP=250 (ΣK=13.046)

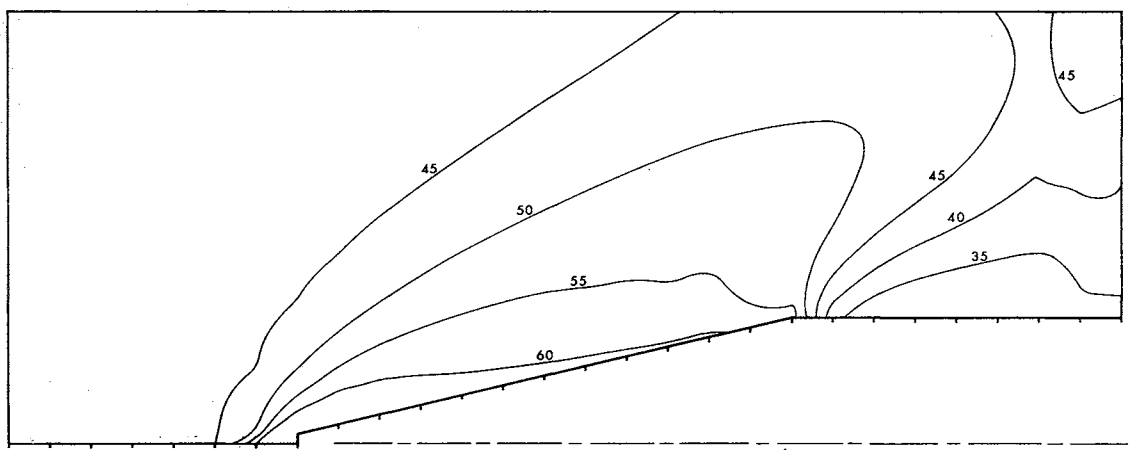

(d) TP=350 (ΣK=18.000)

Figure 12. (continued)

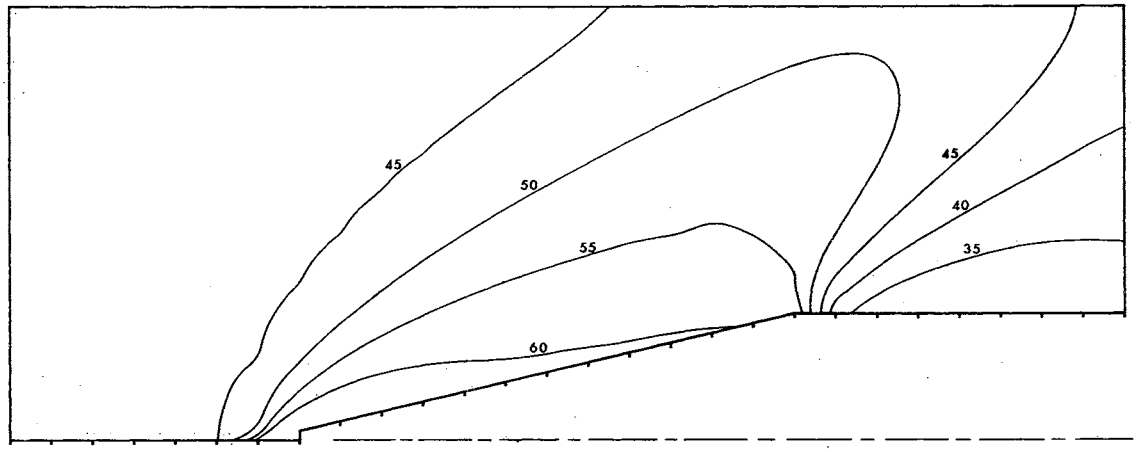

(e) TP=450 (ΣK=23.217)

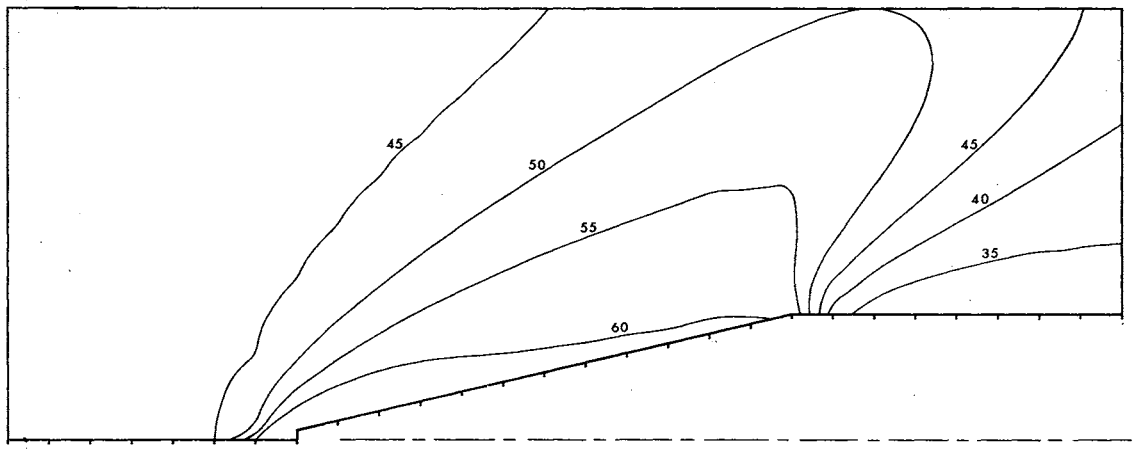

(f) TP=550 (ΣK=28.512)

Figure 12. (continued)

remained practically unchanged for 100 consecutive time planes. The program for the real gas case was run for 550 time planes, or 100 more time planes than the ideal gas case. Data for time planes 450 and 550 are tabulated so that the ideal case can be directly compared with the real gas case, and the final steady state of both cases can be compared to data obtained by other methods. Table III indicates how the results of Phase 1, real and ideal, compare with those given by gas tables, NACA 1135 (28), and Ballistic Research Laboratory (30). The cone-surface pressure is represented in Table III by the pressure which exists at the third surface mesh point upstream from the cone-cylinder intersection; the cylinder pressure is taken from the third mesh point downstream from this junction; and the angle of the bow wave is determined by the angle of the constant pressure curve whose value is the average of the pressures immediately upstream and downstream from the shock. As can be seen from Table III, the numerical results agree well with the standard gas tables and there are no big differences between the real and ideal gas cases.

Phase 1 for ideal gas was also run with an "artificial dissipation" value (ω) of 1.0, which worked well for this phase. The resulting bow shock was not as diffused and the influence of the stagnation point was more confined. But the difficulty with the lower value for the blurring term occurred while calculating Phase 2. The dissipative effect of $\omega = 1.0$ was not great enough to keep the pressure immediately outside the blast sphere from going negative. Once obtained, the negative pressures caused instability which quickly spread throughout the field. Because the value of this parameter affects the conditions of all

TABLE III

COMPARISON OF PHASE 1 STEADY STATE

WITH STANDARD GAS TABLE VALUES

Source of Data	Stagnation Pressure	Cone Surface Pressure	Cylinder Surface Pressure	Bow Wave Angle
Reference 28 and 30	190.0	61.6	30.2	38^{o}
Ideal Gas, TP 450	177.9	62.31	30.08	35^{o}
Real Gas, TP 450	188.8	61.87	29.83	33^{o}
Real Gas, TP 550	187.9	62.83	30.59	37^{o}

steady states, $\omega = 1.5$ was used to obtain the final results in all phases, even though with this value the Phase 1 steady-state results were more diffused.

Phase Two Results

The anticipated transient state shock patterns for Phase 2 are given in Figure 2, ("b" and "c"). These results are the same as those predicted by Wolff (1) for shocks with zero thickness, i.e., the shock thickness is much smaller than any other significant configuration dimension. This is not the case with solutions obtained by numerical methods. In most instances, normal shock waves are diffused over a region of approximately three to four mesh points. In this study, however, the total length of the cone for all three phases is twelve mesh points. Thus the thickness of the diffused shock is approximately 30% of the total length of the cone. By expanding the normal and oblique shocks of Figure 2b over a finite distance and representing them by isobars, Figure 13 was obtained. This figure shows the type of result which can be expected by numerical techniques when the distance between two mesh points is one order of magnitude less than the total cone length.

The numerical results of this phase are given by Figure 14. Figure 14, Parts "e" and "f", which show the transient flow, do in fact compare favorably with Figure 13. The new bow shock can be seen developing as the normal shock front passes over and the flow field downstream from the shock front is essentially unchanged. Although the details of the transient interactions are lost because of the restricted

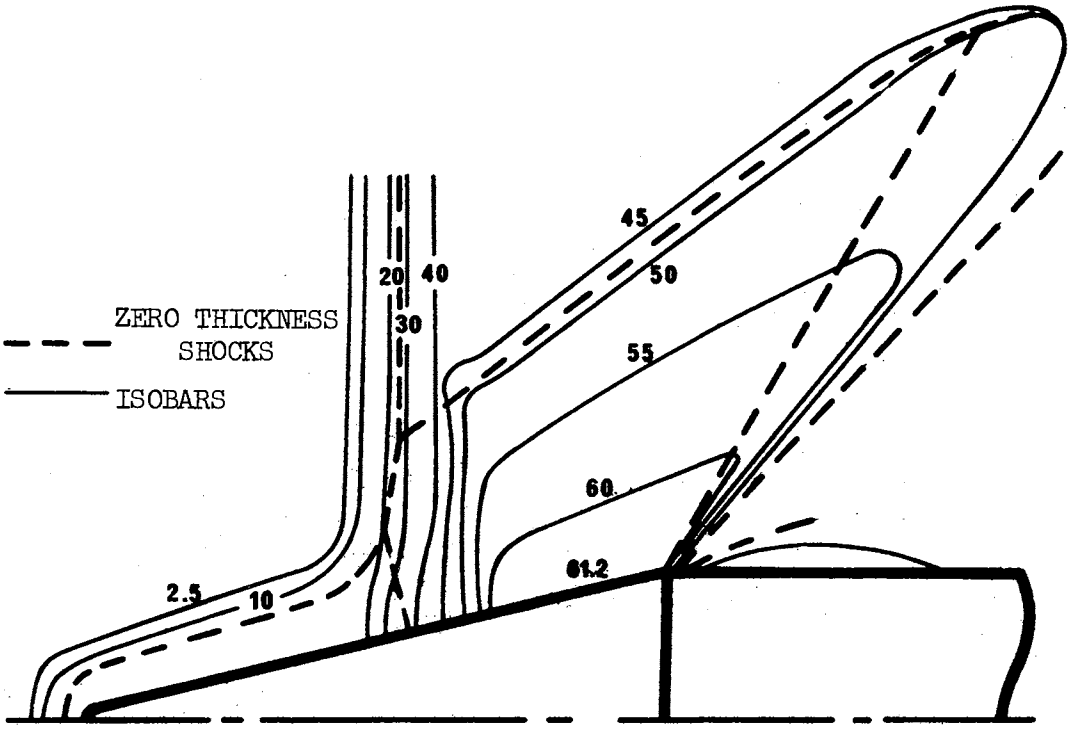

Figure 13. Effect of Finite Shock Thickness on Phase 2

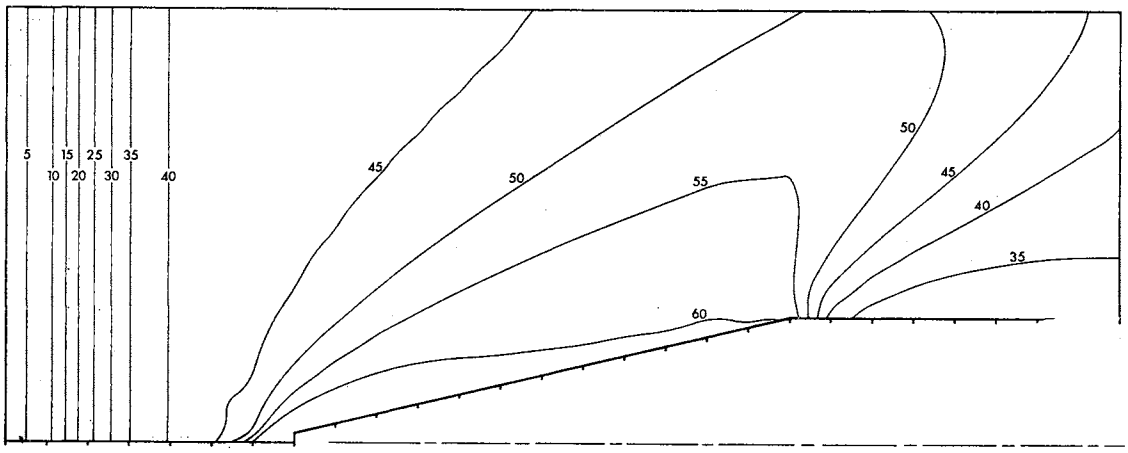

(a) TP=50 (ΣK=1.944)

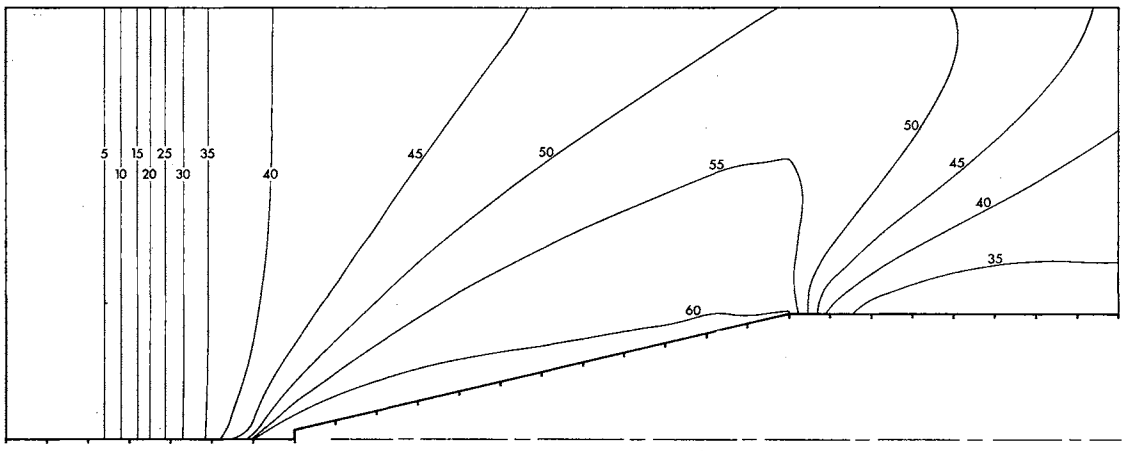

(b) TP=100 (ΣK=3.888)

Figure 14. Constant Pressure Lines for Phase 2: Cone-Cylinder Exiting From Blast Sphere (Initial Conditions are given in Table II)

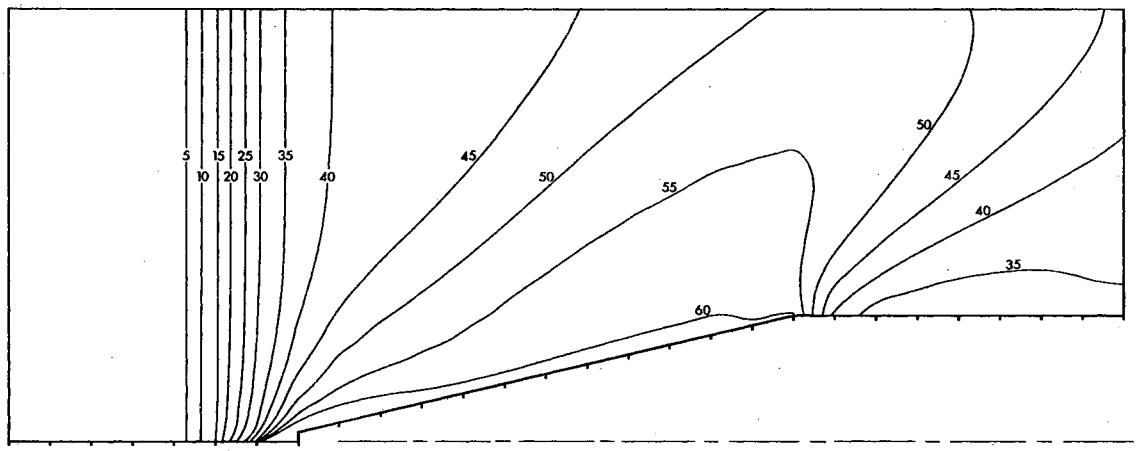

(c) TP=150 (ΣK=5.776)

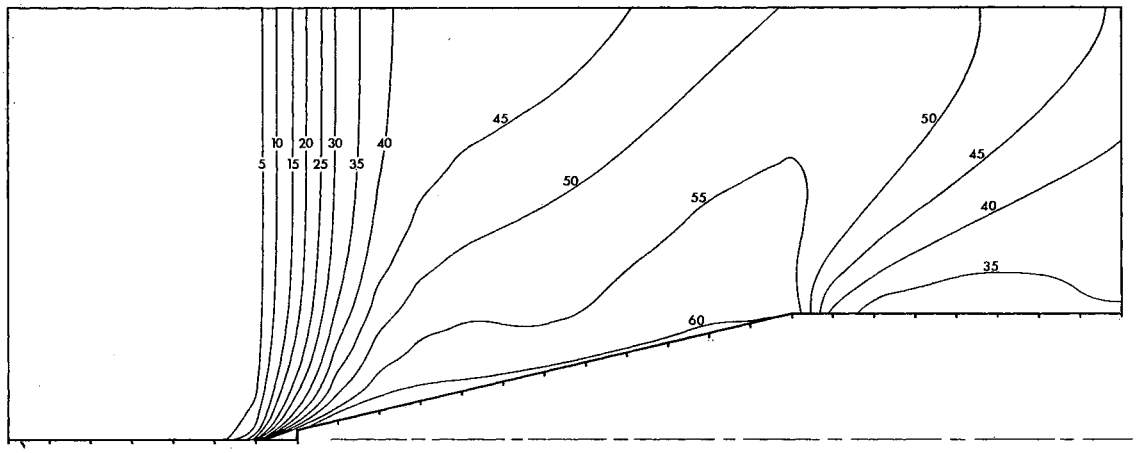

(d) TP=200 (ΣK=7.634)

Figure 14. (continued)

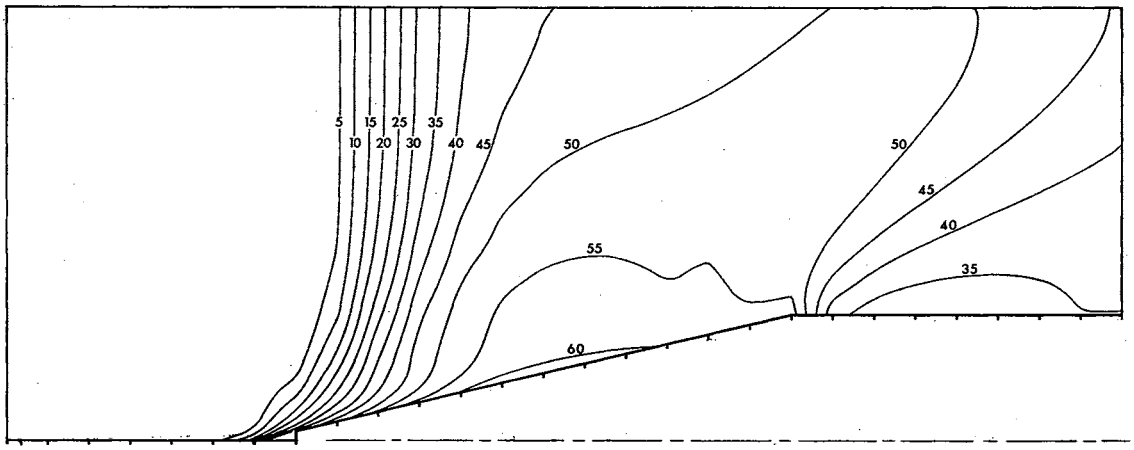

(e) TP=250 (ΣK=9.516)

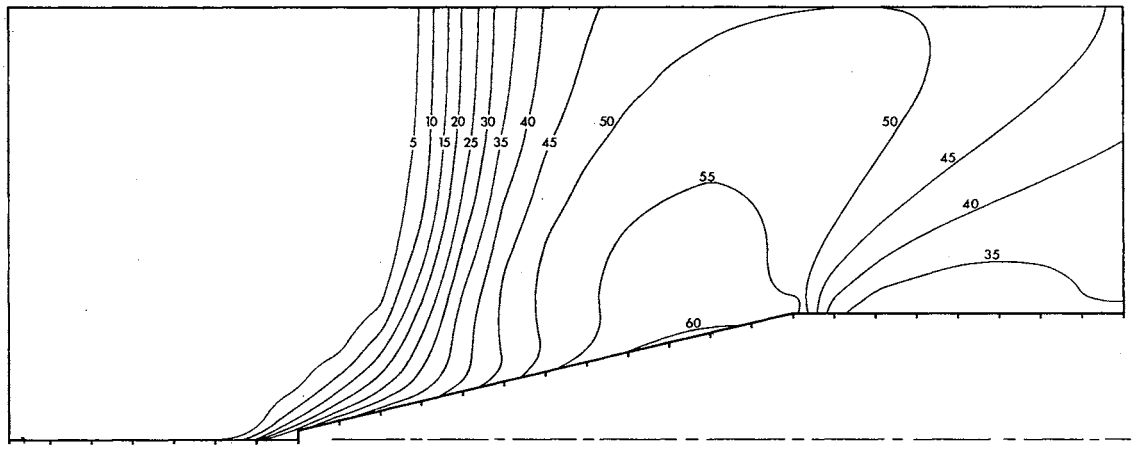

(f) TP=300 (ΣK=11.402)

Figure 14. (continued)

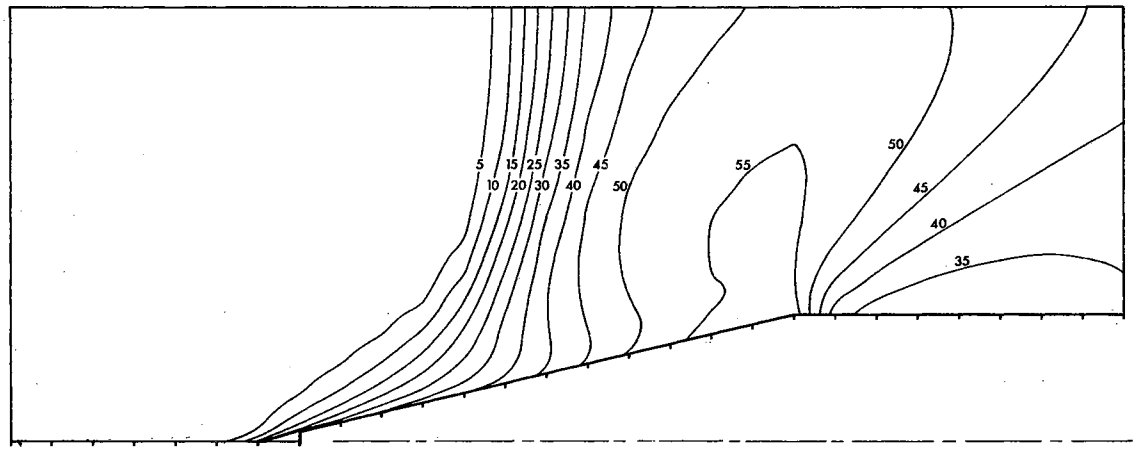

(g) TP=350 (ΣK=13.282)

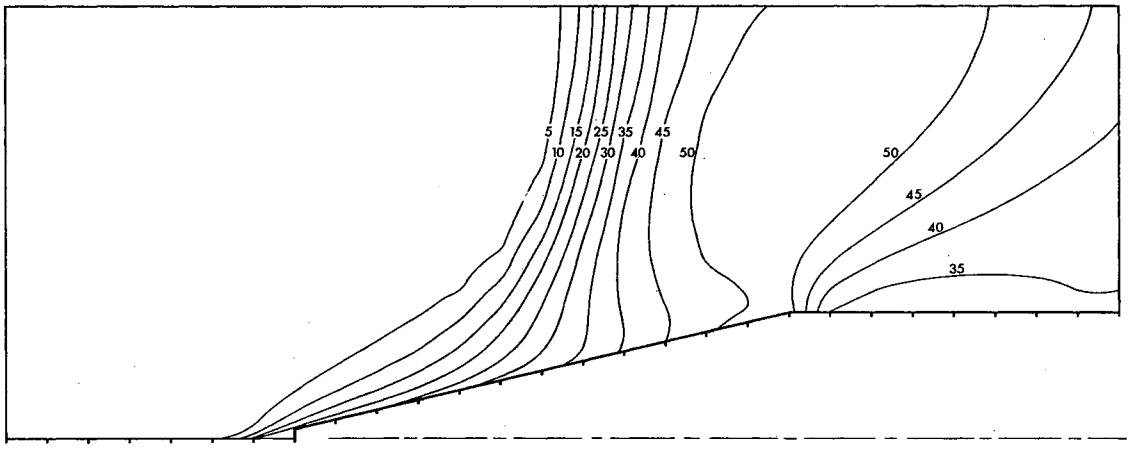

(h) TP=400 (ΣK=15.162)

Figure 14. (continued)

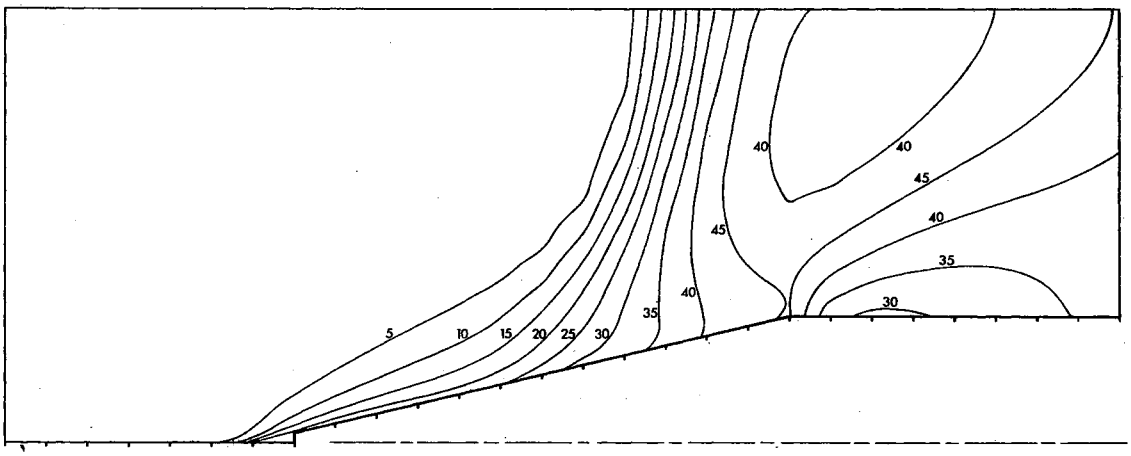

(i) TP=450 (ΣK=17.046)

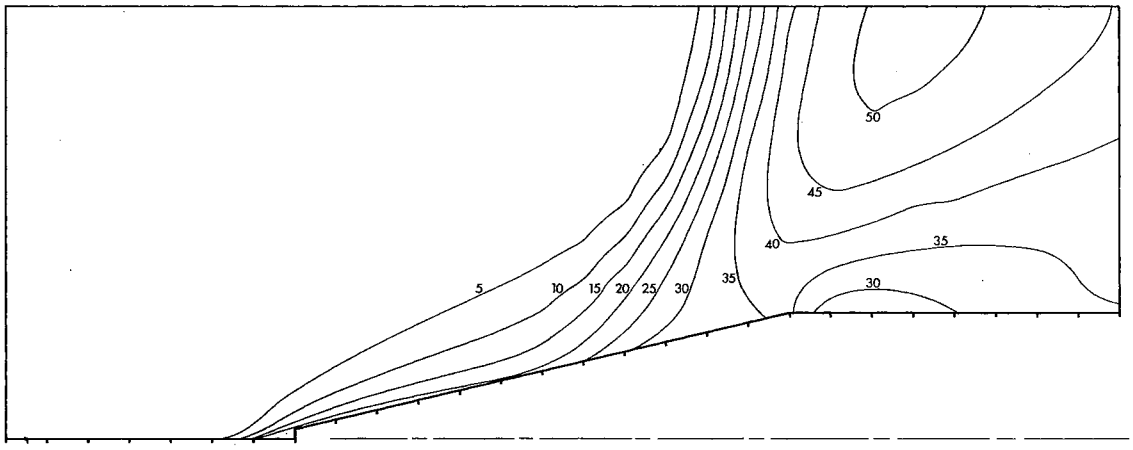

(j) TP=500 (ΣK=18.930)

Figure 14. (continued)

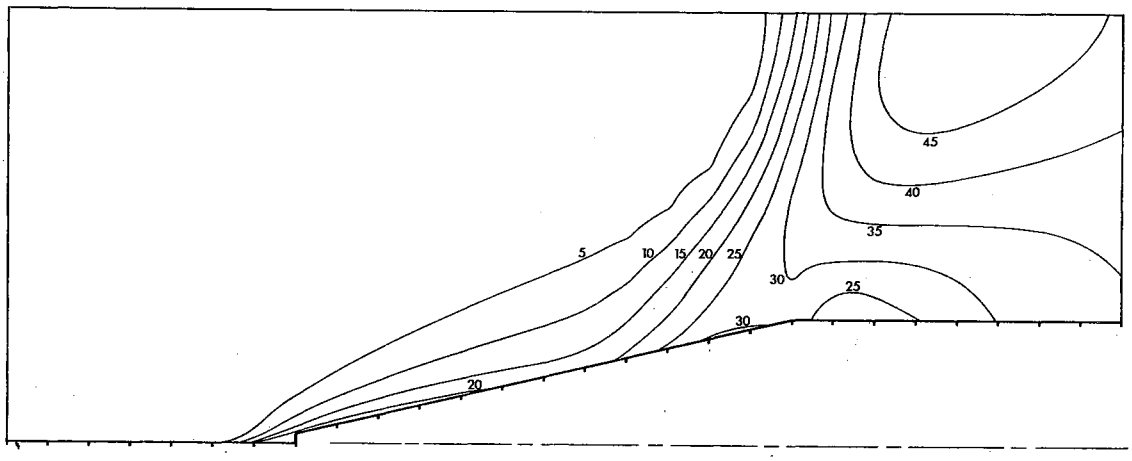

(k) TP=550 (ΣK=20.822)

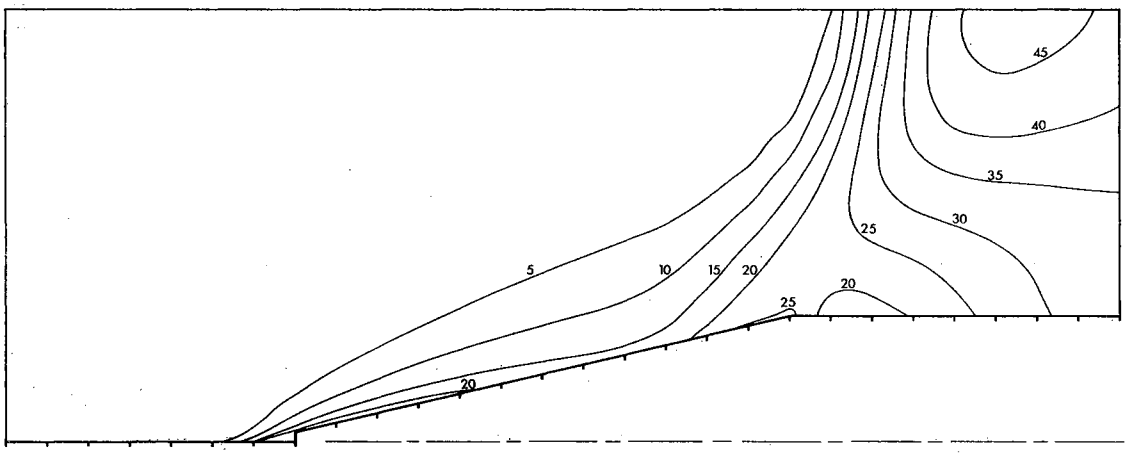

(ℓ) TP=600 (ΣK=22.715)

Figure 14. (continued)

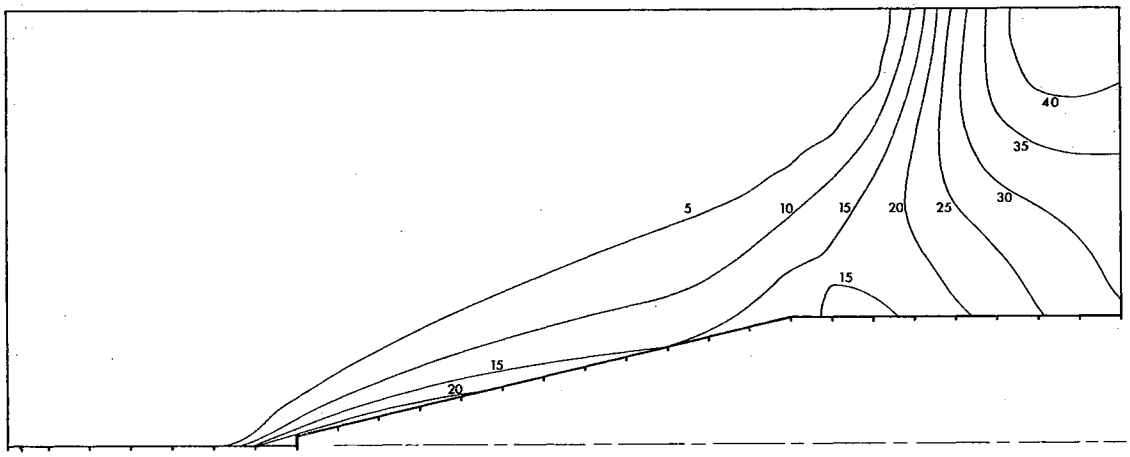

(m) TP=650 (ΣK=24.619)

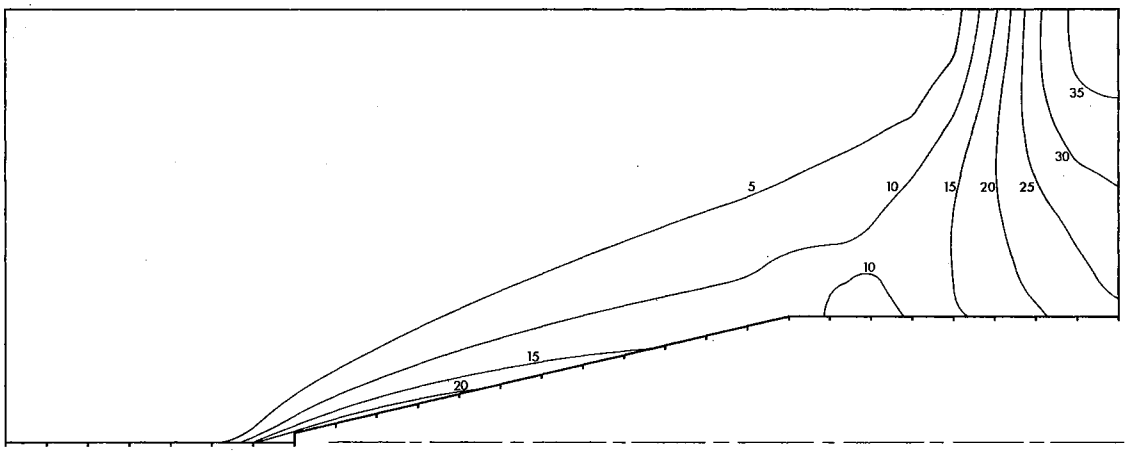

(n) TP=700 (ΣK=26.528)

Figure 14. (continued)

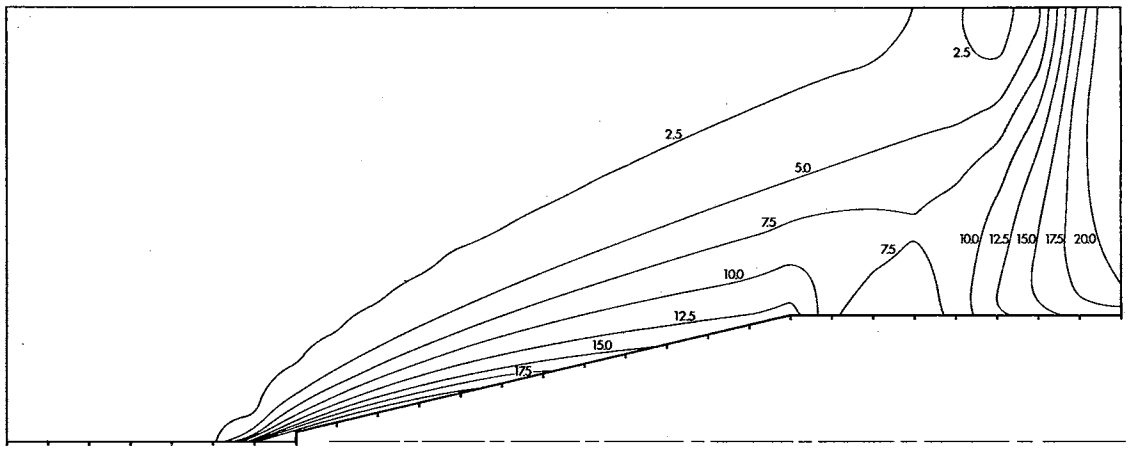

(o) TP=750 (ΣK=26.442)

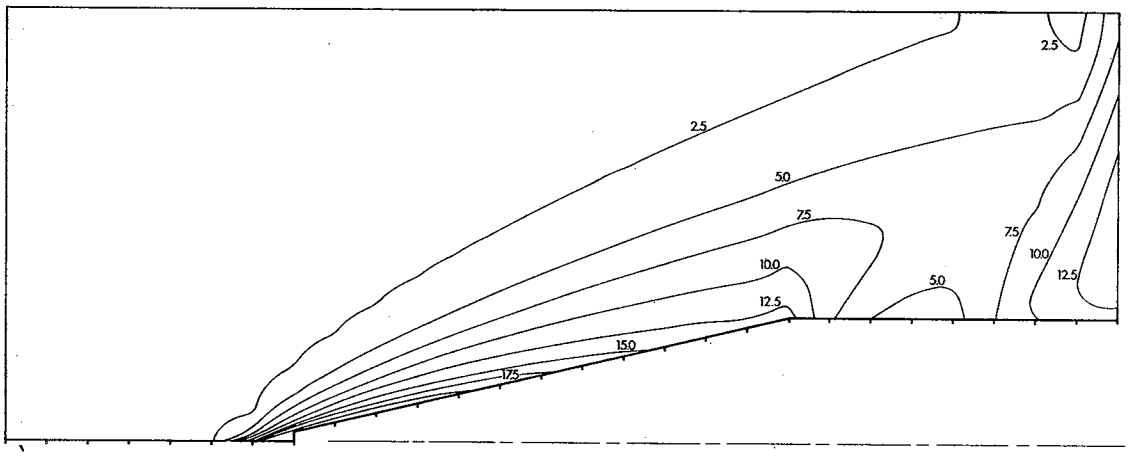

(p) TP=800 (ΣK=30.361)

Figure 14. (continued)

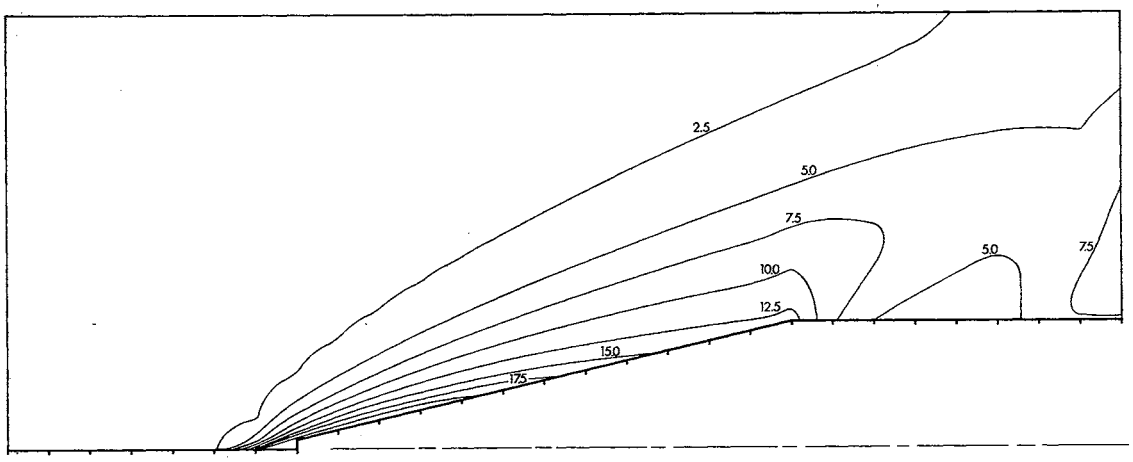

(q) TP=850 (ΣK=32.289)

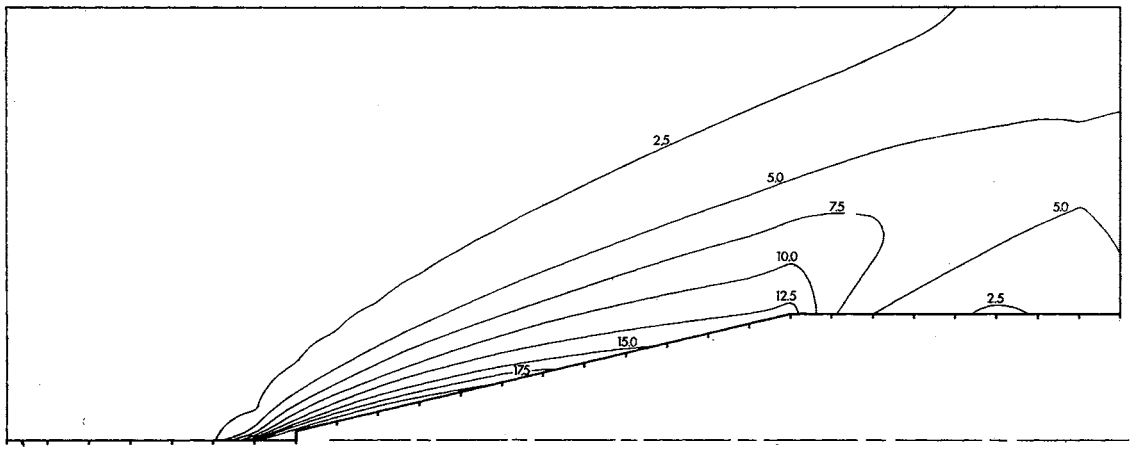

(r) TP=900 (ΣK=34.214)

Figure 14. (continued)

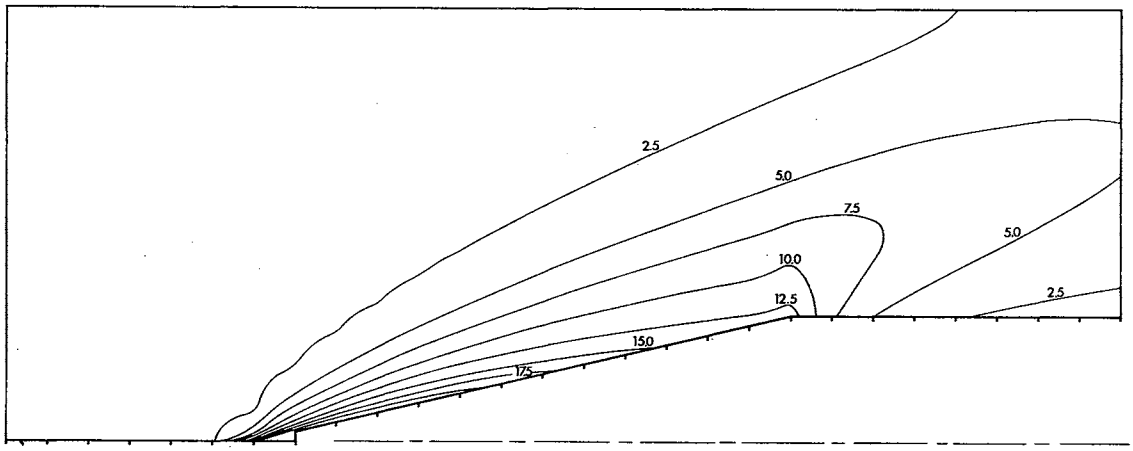

(s) TP=950 (ΣK=36.135)

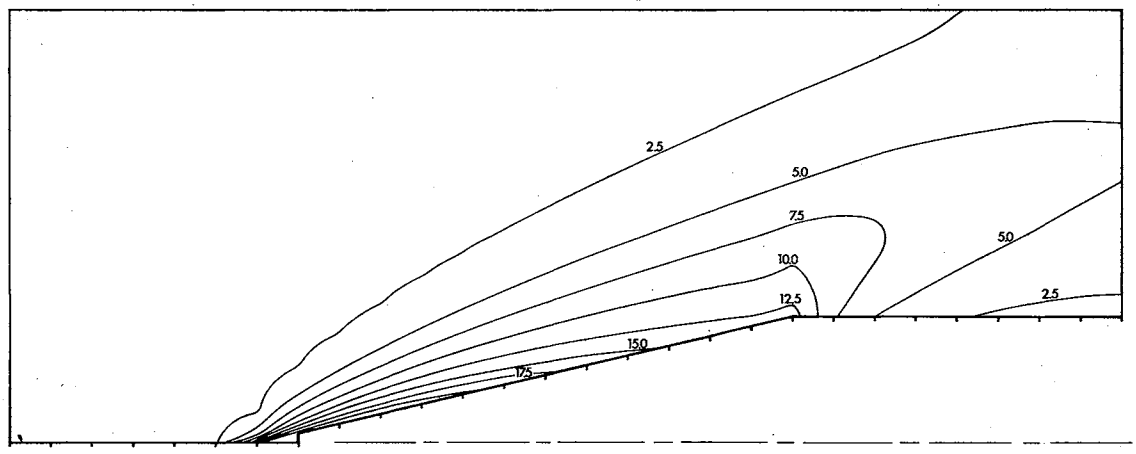

(t) TP=1000 (ΣK=38.055)

Figure 14. (continued)

number of mesh points, the three shocks (normal shock front, old bow wave, and new bow wave) blend together in a manner similar to Figure 13.

Phase 2 requires that a large number of time planes be calculated to obtain a steady state. Since the actual time increment between time planes is determined in part by $(v+w)^{-1}_{max}$ and the maximum velocity (v) existing in the flow field is high, the time step (τ) is small. The relative movement of the shock front with respect to the body is also quite slow so that the interaction takes place over a long period of time. Although high velocities with respect to the ground are involved, the projectile is relatively slow in moving through the blast front, which is traveling in the same direction as the body. A total of 1001 time planes were run for Phase 2. The maximum pressure change between the 1000th time plane and the 1001th time plane was less than 0.12%. With more time planes, the percentage change could have been reduced; however, the cost of computer time could not justify additional computations. A better steady-state shock wave was obtained for this case than Phase 1; Figure 14, Parts "r", "s", and "t" which portray a time differential of 100 time planes, indicate that the shape of the bow wave is fixed. Also, the pressure flow field has become steady with time.

The vital statistics of the Phase 2 steady state are given in Table IV. The cone surface pressure is taken three mesh points upstream from the cone-cylinder junction, and the cylinder pressure is taken seven mesh points downstream. The cone pressures for both cases were nearly the same and the shock angles were equal. The shock angle, that angle maintained by the constant pressure line of 6.05, represents

TABLE IV

COMPARISON OF PHASE 2 STEADY STATE WITH

STANDARD GAS TABLE VALUES

Source of Data	Stagnation Pressure	Cone Surface Pressure	Cylinder Surface Pressure	Bow Wave Angle
Reference 28 and 30	136.0	11.1	1.57	17.2°
Ideal Gas, TP 1000	169.3	14.40	1.591	20.5°
Real Gas, TP 1000	191.9	14.69	1.717	20.5°

one-half of the pressure rise across the shock. The free stream Mach number of this phase for real gas is 6.9; therefore, the flow approaches the hypersonic regime. The largest difference between the real gas and ideal gas occurs at the stagnation point. Use of the assumption that the sonic velocity was equal to $\sqrt{\gamma p/\rho}$ resulted in a larger Mach number for the real gas case at the first mesh point upstream from the nose. Consequently, when the flow was isentropically stagnated, the resulting stagnation pressure was larger. The larger free stream Mach number of Phase 2 forced the shock wave closer to the cone nose. As a result, the first mesh point upstream from the nose did not experience the proper entropy increase nor stagnation pressure loss.

So that the influence which the cone-cylinder has on the flow region upstream from this junction could be determined, the cone was extended five mesh points, and a new Phase 2 steady state was obtained. The pressure at the previous cone-cylinder intersection increased 3%; the next surface point upstream increased 1.5%; and all other surface points changed less than 1.0%. The surface pressure on the extended portion of the cone continued to decrease asymptotically toward the theoretical pressure of 11.1.

Phase Three Results

The steady-state results of Phase 2 provided a satisfactory set of initial data for Phase 3. The results of Phase 3 are given in Figure 16. This phase simulates a cone-cylinder configuration entering a blast front from an undisturbed atmosphere. For shocks of zero thickness, the results anticipated by Wolff (1) for the transient state of this phase

are shown in Figure 1b, and the anticipated results for a numerical solution are given in Figure 15. This figure was obtained by expanding the normal and oblique shock waves in Figure 1b over a finite distance. Although the computer limitations restrict the amount of detail that can be expected, the pressure profiles illustrated in Figure 15 resemble the numerical results achieved (Figure 16b) in the following ways. As the normal shock passes over the projectile, a new bow shock is formed and the portion of the original bow shock downstream from the normal shock remains essentially unchanged. The new pressure levels imposed along the cone surface, while the normal shock passes over, are approximately the same levels as those maintained after steady-state conditions are achieved. The detail is insufficient to observe the sonic circle as predicted by Smyrl (10).

A steady-state condition was obtained in which the pressure change between the time planes 550 and 551 was no more than 0.3%. Although the bow wave was stabilized, the larger changes occurred toward the right boundary. Because the final data were not to be used as initial data for future phases, additional time planes were not computed. Table V gives the steady-state properties of Phase 3. The cone-surface pressure was taken from the third surface mesh point in front of the cone-cylinder intersection; the cylinder pressure was taken seven mesh points downstream. The constant pressure line of 80, which represents one-half the pressure rise across the shock, was used to represent the bow shock angle. The large free stream Mach number of 4.96 forces the portion of the bow shock which lies at the axis of symmetry to move within one mesh point of the nose. Consequently, the reduced entropy

rise which occurs at the stagnation point is very nearly the same as that which occurred in Phase 2. As Table V shows, the surface pressure correlation becomes worse close to the stagnation point. While the error in pressure on the cylinder is less than 10% the stagnation point error is greater than 45%. This correlation substantiates the concept that part of the bow shock is within one mesh point of the cone nose.

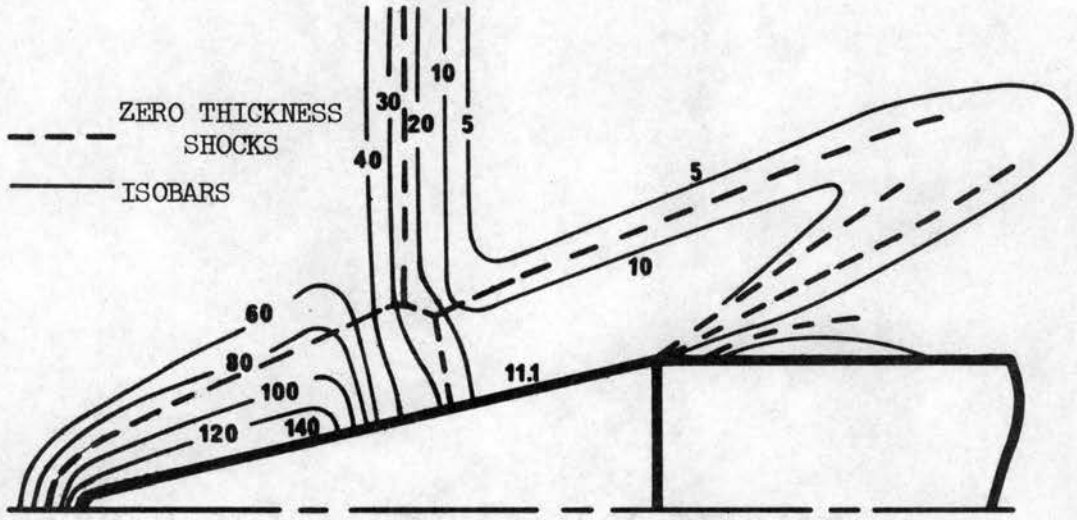

Figure 15. Effect of Finite Shock Thickness on Phase 3

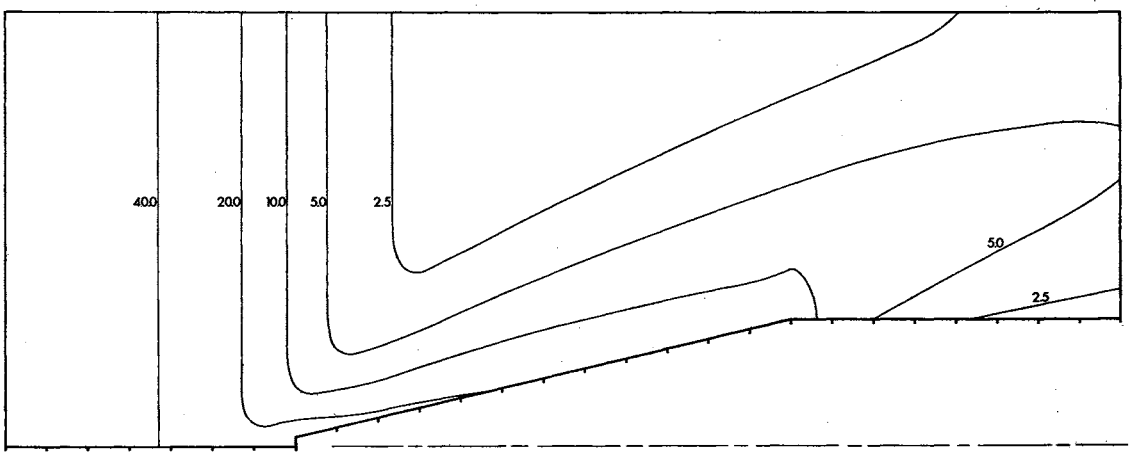

(a) TP=50 (ΣK=1.253)

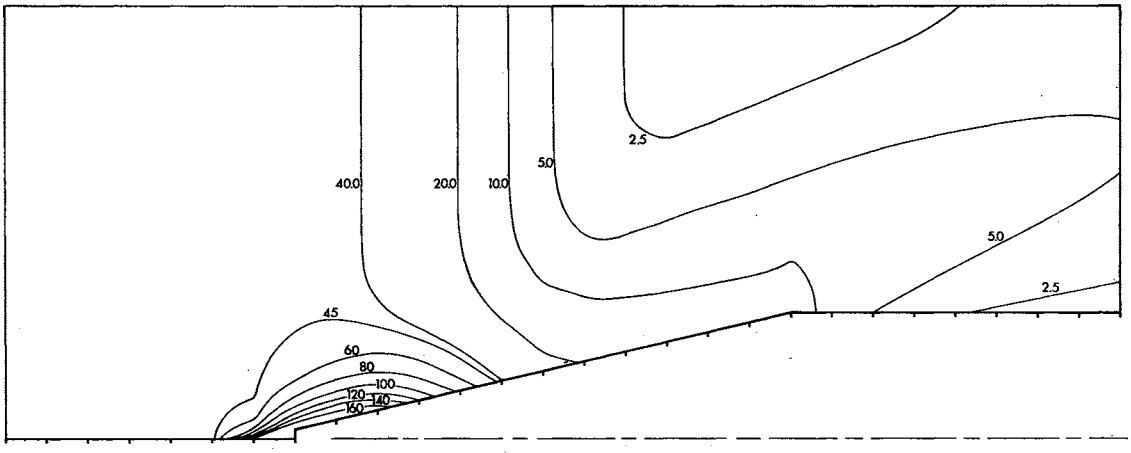

(b) TP=100 (ΣK=2.497)

Figure 16. Constant Pressure Lines for Phase 3: Cone-Cylinder Entering Blast Sphere (Initial Conditions are given in Table II)

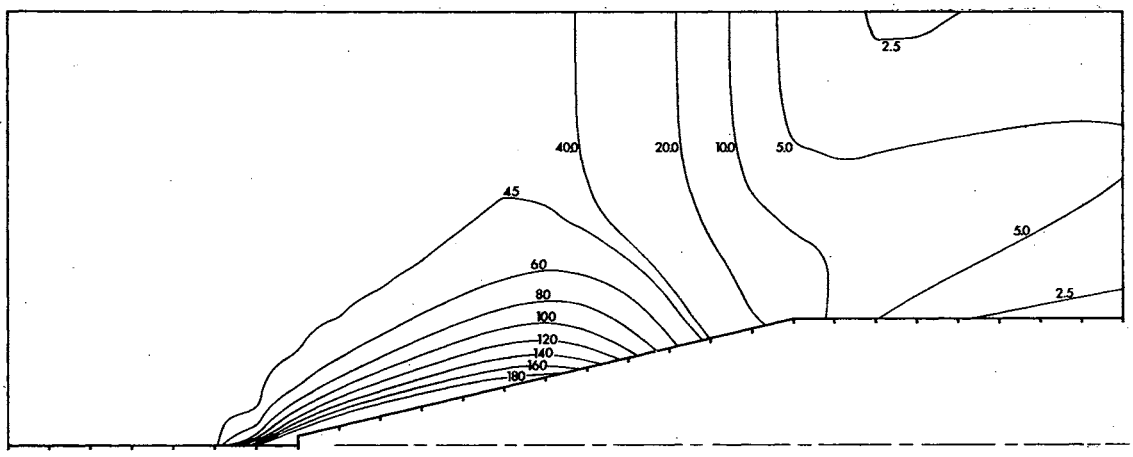

(c) TP=150 (ΣK=3.739)

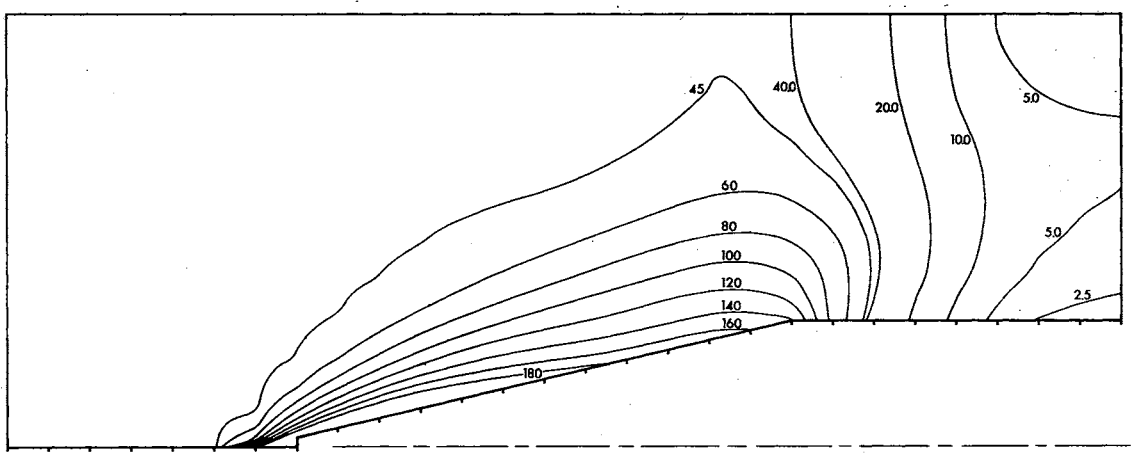

(d) TP=200 (ΣK=4.977)

Figure 16. (continued)

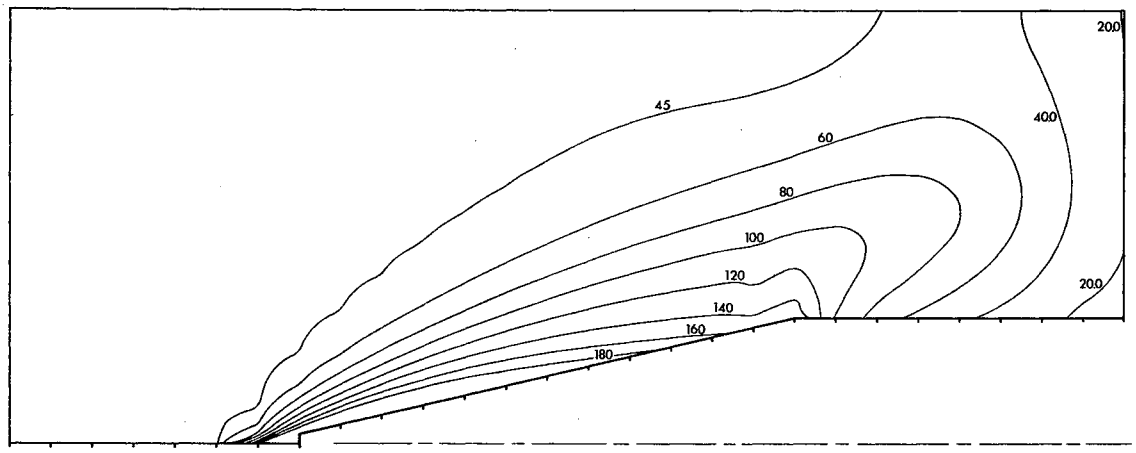

(e) TP=250 (ΣK=6.204)

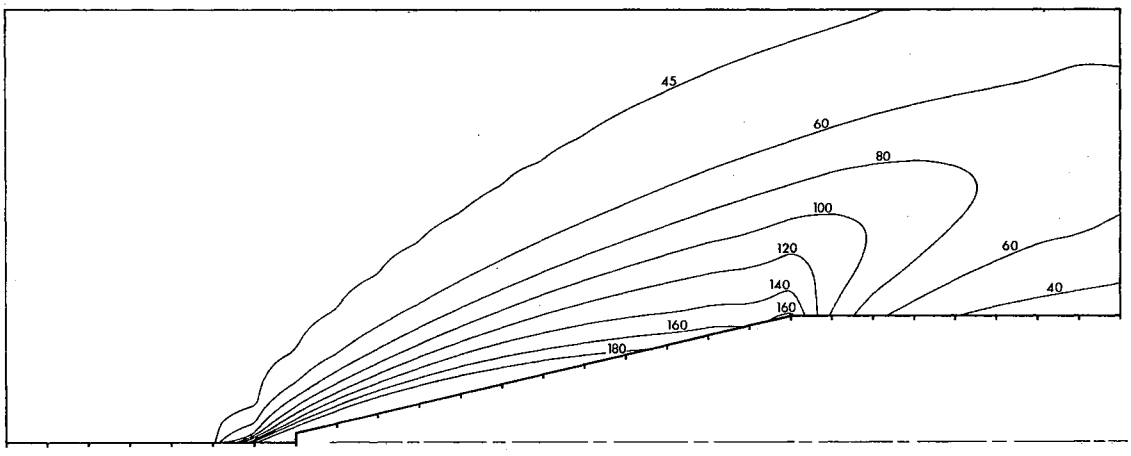

(f) TP=300 (ΣK=7.402)

Figure 16. (continued)

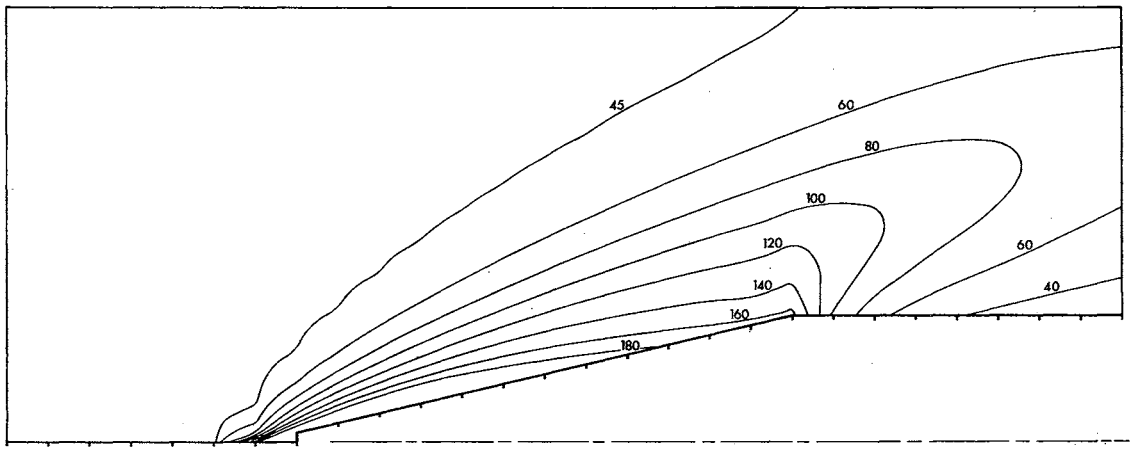

(g) TP=350 (ΣK=8.635)

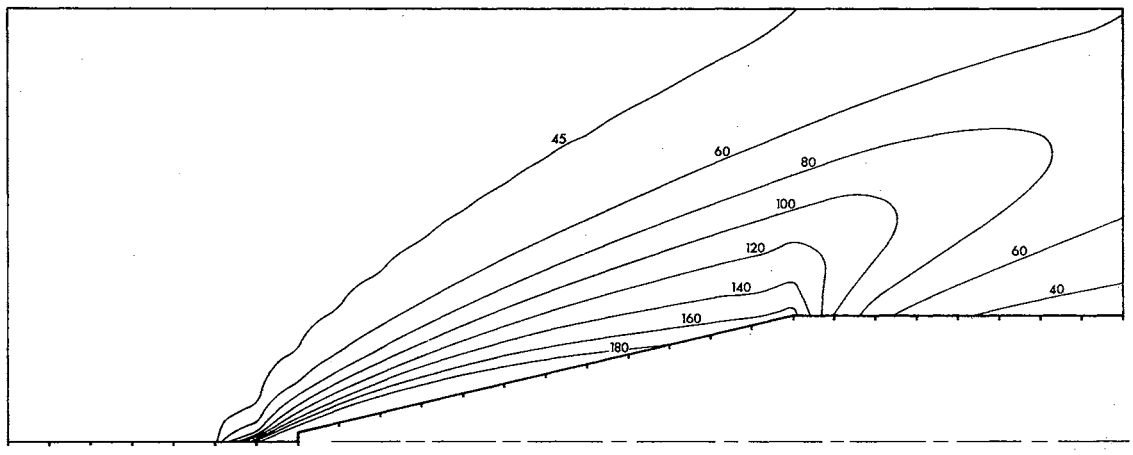

(h) TP=400 (ΣK=9.884)

Figure 16. (continued)

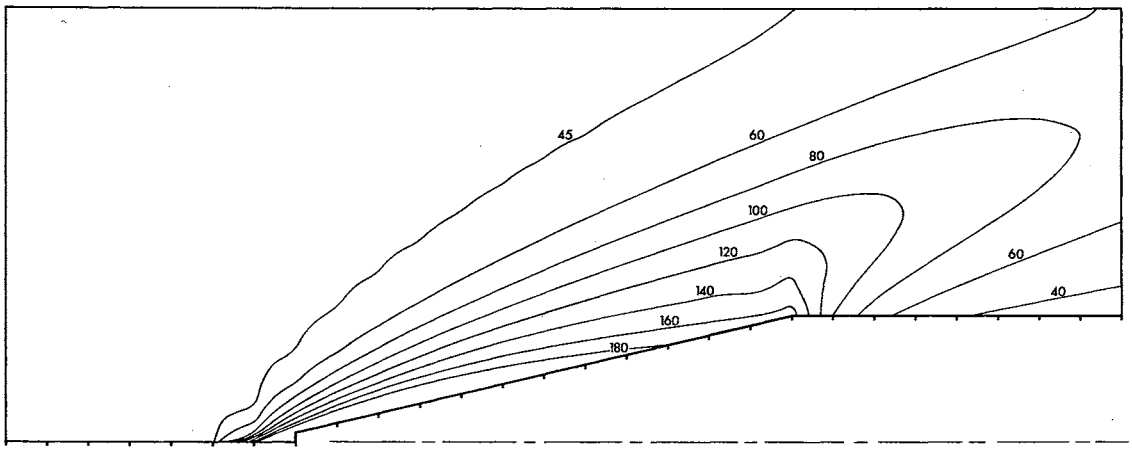

(i) TP=450 (ΣK=11.139)

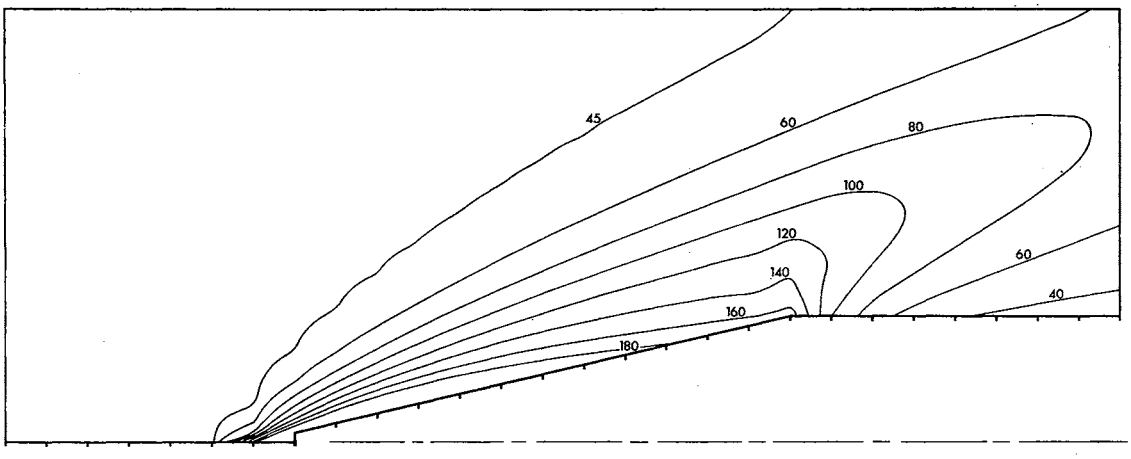

(j) TP=500 (ΣK=12.393)

Figure 16. (continued)

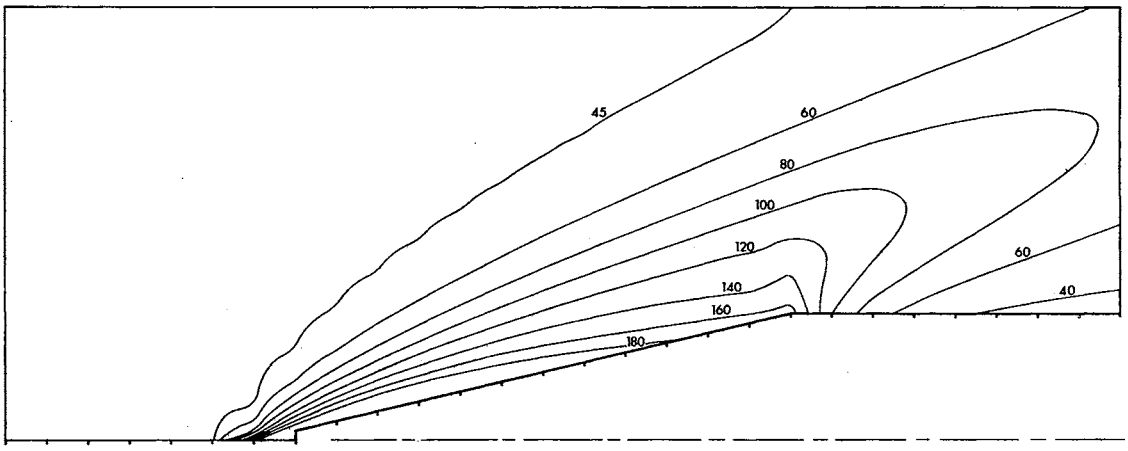

(k) TP=550 (ΣK=13.648)

Figure 16. (continued)

TABLE V

COMPARISON OF PHASE 3 STEADY STATE WITH

STANDARD GAS TABLE VALUES

Source of Data	Stagnation Pressure	Cone Surface Pressure	Cylinder Surface Pressure	Bow Wave Angle
Reference 28 and 30	1420.0	140.6	30.7	18.3°
Real Gas, TP 550	2093.4	180.0	32.93	22.0°

CHAPTER VI

CONCLUSIONS AND RECOMMENDATIONS

Conclusions

The primary objective of devising a method by which flow about a cone-cylinder configuration can be obtained has been accomplished. The results show that the impulse received upon an entering body is of such a nature as to cause the body to implode; while the body, upon exiting from the blast front, would have a tendency to explode. For the case presented having a blast pressure ratio of 20, the pressure ratio change on the cone surface is greater than 12 after entering and less than 6 upon exiting. Although the larger pressure ratio imposed upon the entering cone-cylinder appears to be more extreme, the sudden decrease in pressure that occurs during the exiting phase might be the more difficult design requirement. For the 13.347 degree cone, there were no local transient pressure pulses which exceeded the steady-state pressure values.

Several conclusions may be drawn from the use of the numerical techniques. The conditions imposed on the boundaries of the mesh point array are extremely important, for the manner in which they are treated greatly affects the properties obtained at the boundaries, and, consequently, can have an effect on the entire flow field. The final technique which was used at the stagnation point always gave stable

results. Consequently, this method is completely adequate for computations, where the free stream Mach number is 1.7. But, where the free stream Mach numbers were higher, the results were less accurate. The problem of obtaining accurate stagnation properties becomes even more acute as the cone apex angle decreases so that the ratio of the stagnation pressure to the cone surface pressure increases. Thus, the larger this ratio, the larger the cone surface pressure error. For studies involving Mach numbers greater than 1.7, additional numerical techniques must be developed for the stagnation point region.

The cone surface boundary was one of the most complex mathematical aspects of the study. Although several different techniques provided stable results, none was completely acceptable. The applied method yielded surface pressures which were too large with respect to the surrounding field points. The result was a slight distortion of the pressure field close to the cone surface. This inconsistency was attributed to the use of forward differences on the cone surface.

The numerical treatment of the right boundary was not as critical as the treatment imposed on other boundaries. An impulse created at the boundary when it is poorly treated does not propagate upstream any appreciable distance. This result was not entirely unexpected because the mesh points of interest lie at the downstream edge of a supersonic flow field. The upper boundary was treated in a fashion similar to the right boundary and this treatment proved to be satisfactory. However, the technique used at this location was critical because its effects could be propagated to other parts of the flow field. The results at this boundary were reasonable, as well as stable, under all transient

conditions. There is a tendency for the constant pressure lines in the region of strong pressure gradients to bend slightly forward, indicating that the border pressures in this region are somewhat high. The inconsistency in this case was again attributed to the application of the "off-centered", or "backward" differencing method.

The numerical technique remained stable when the constant specific heat ratio (γ) was replaced by a curve-fitted variable. Thus the numerical solution is good not only for an ideal gas but also for a real gas in equilibrium. Consequently, results can be obtained for conditions under which the ideal gas equation of state fails. There was very little difference between the real gas case computed and the ideal gas. Although the flow properties varied a small percentage, the resulting shock patterns were almost identical.

Additional detail could be obtained by use of the numerical technique if a much larger number of mesh points were used, so that the effective width of the shock became smaller. If the number of mesh points in each direction were increased by a factor of three, the results would be far superior. Not only would this require a computer with a much larger memory, but it would also be preferable to have a faster machine. The suggested increase in the quantity of mesh points would increase the computing time by a factor of approximately nine. On the IBM 7040 computer, the time required to compute a case would then be approximately one hundred hours.

Recommendations

Based upon the information obtained from this study, the following

recommendations are made:

1. An investigation should be conducted to develop a mesh point system that would not include the stagnation point. One such technique is currently used by Mr. Ken Royer in his study of boundary layer shock interaction for viscous flow. The mesh point array is arranged so that the center line of the cone lies half-way between two rows of mesh points; thus, no direct calculation needs to be done for the stagnation point.
2. If a larger and faster computer were available, the problem could be re-run using the original mesh system or the one recommended above. By using the maximum feasible number of mesh points, a solution with more detail could be obtained. The ideal solution would be one in which the effective width of a shock would be insignificant with respect to all other typical configuration dimensions.
3. The configuration investigated in this study was a two-dimensional (r,z) axi-symmetric problem. The theory might be extended to three dimensions (r,z,Φ) so that the movement of the oncoming blasts would not be restricted to the direction of the axis of symmetry.

A SELECTED BIBLIOGRAPHY

1. Wolff, W. S., "Transient Flow Field Analysis Around a Conical Body Exposed to a Blast Wave," Lockheed Corp. Report LMSC No. 4-70-64-1, 1964.

2. Von Neumann, J., and R. D. Richtmyer, "A Method for the Numerical Calculation of Hydrodynamic Shocks," J. Appl. Physics, Vol. 21, 1950, p. 232.

3. Rusanov, V. V., "The Calculation of the Interaction of Non-Stationary Shock Waves and Obstacles," National Research Council of Canada Library, Ottawa, Canada, Tech. Translation 1027 by D. A. Sinclair, 1962. Translated from: Zhurnal Vychislitelnoi Fiziki, Akademiya Nauk, SSSR 1, Vol. 1, No. 2, 1961, pp. 267-279.

4. Tyler, L. D., "Numerical Solutions of the Flow Field Produced by a Plane Shock Wave Emerging into a Crossflow," Ph.D. Dissertation, Oklahoma State University, May, 1965; Published as Eng. Res. Rpt. SBW-10 by Tyler, L. D., and Zumwalt, G. W., 1965.

5. Jackomis, W. N., "Transient Flow Field Analysis of a Plane Blast Wave Intercepting a Stationary Cone at Zero Angle of Attack," Ph.D. Dissertation, Oklahoma State University, May, 1965; Published as Eng. Res. Rpt. SBW-9 by Jackomis, W. N., and Zumwalt, G. W., August, 1965.

6. Walker, W. F., "A Numerical Solution for the Interaction of a Moving Shock Wave with a Turbulent Mixing Region," Ph.D. Dissertation, Oklahoma State University, May, 1966.

7. Walker, W. F., and L. D. Tyler, "Literature Survey on Shock Wave Interactions with Shocks and Bodies," Oklahoma State University Report SBW-7, Oct., 1964.

8. Lighthill, M. J., "The Diffraction of Blast I," Proc. Roy. Soc., Series A, Vol. 198, 1949, p. 454.

9. Chester, W., "The Diffraction and Reflection of Strong Waves," Quart. Mech. and Applied Math., Vol. 7, Part 1, 1957.

10. Smyrl, J. L., "The Impact of a Shock-Wave on a Thin Two-Dimensional Aerofoil Moving at Supersonic Speeds," J. Fluid Mech., Vol. 15, 1963, p. 223.

11. Blankenship, V. D., "Shock-Shock Interaction on a Slender Supersonic Cone," J. Fluid Mech., Vol. 22, Part 3, pp. 599-615.

12. Whitham, G. B., "A New Approach to Problems of Shock Dynamics, Part I, Two-Dimensional Problems," J. Fluid Mech., Vol. 2, 1957, p. 145.

13. Whitham, G. B., "On the Propagation of Shock Waves Through Regions of Non-Uniform Area or Flow," J. Fluid Mech., Vol. 4, 1958, p. 337.

14. Whitham, G. B., "A New Approach to Problems of Shock Dynamics, Part 2, Three-Dimensional Problems," J. Fluid Mech., Vol. 5, 1959, p. 369.

15. Miles, J. W., "A Note on Shock-Shock Diffraction," J. Fluid Mech., Vol. 22, Part 1, 1964, pp. 95-102.

16. Burstein, S. Z., "Finite Difference Calculations for Hydrodynamic Flows Containing Discontinuities," AEC Computing and Applied Mathematics Center, Courant Institute of Mathematical Sciences, New York University, Mathematics Report NYO-1480-33, 1965.

17. Holt, M., Basic Developments in Fluid Dynamics, Academic Press, New York and London, Vol. 1, 1965.

18. Richtmyer, R. D., "A Survey of Difference Methods for Non-Steady Fluid Dynamics," NCAR Technical Notes 63-2.

19. Gary, J., "On Certain Finite Difference Schemes for the Equations of Hydrodynamics," TID-4500, 16th Ed., NYO-9188, Physics AEC Computing and Applied Mathematics Center, Courant Institute of Mathematical Sciences, New York University, 1964.

20. Merritt, D. L., and P. M. Aronson, "Free Flight Shock Interaction Studies," AIAA Paper No. 66-57, 1966.

21. Brown, E. A. and G. J. Mullaney, "Technique for Studying the Shock-on-Shock Problem," AIAA Journal, Vol. 3, No. 11, 1965, pp. 2167-2168.

22. Brown, E. A. and G. J. Mullaney, "Experiments on the Head-On Shock-Shock Interaction," AIAA Journal, Vol. 3, No. 11, 1965, pp. 2168-2170.

23. Bryson, A. E., and R. W. F. Gross, "Diffraction of Strong Shocks by Cones, Cylinders, and Spheres," J. Fluid Mech., Vol. 10, 1961, p. 1.

24. Klein, E. J., "Interaction of a Shock Wave and a Wedge: An Application of the Hydraulic Analogy," AIAA Journal, Vol. 3, 1963, p. 801.

25. Godunov, S. K., "A Difference Method for the Numerical Calculation of Discontinuous Solutions of Hydrodynamic Equations," Mathematicheskii Sbornik, Vol. 47, No. 3, 1959, p. 271.

26. Fox, L., Numerical Solution of Ordinary and Partial Differential Equations, Addison Wesley, Reading, Massachusetts, 1962.

27. Doan, L. R., and G. H. Nickel, "A Subroutine for the Equation of State of Air," Air Force Weapons Laboratory, Technical Memorandum No. RTD (WLR) TM-63-2, 1963.

28. Ames Research Staff, "Equations, Tables, and Charts for Compressible Flow," NACA 1135, 1953.

29. Wittliff, C. E., and J. T. Curtis, "Normal Shock Wave Parameters in Equilibrium Air," Cornell Aeronautical Laboratory, Inc., Report No. CAL-111, 1961.

30. Clippinger, R. F., J. H. Giese, and W. C. Carter, "Tables of Supersonic Flows about Cone-Cylinders Part I: Surface Data," Ballistic Research Laboratories, Report No. 729, 1950.

APPENDIX A

TRANSFORMATION OF BLURRING TERMS

The dissipative terms for two-dimensional rectangular coordinates given in Chapter III, equation (3-7), are

$$\frac{\partial(A\frac{\partial f}{\partial x})}{\partial x} + \frac{\partial(B\frac{\partial f}{\partial y})}{\partial y} . \tag{A-1}$$

It may be noted that A = B, and were distinguished earlier for clarity in subsequent algebraic steps. By expanding this concept to three dimensions, the equation becomes

$$\frac{\partial(A\frac{\partial f}{\partial x})}{\partial x} + \frac{\partial(A\frac{\partial f}{\partial y})}{\partial y} + \frac{\partial(A\frac{\partial f}{\partial z})}{\partial z} . \tag{A-2}$$

In order to represent these "dissipation" terms in cylindrical coordinates, a transformation is made using

$$x = r \cos \theta, \; y = r \sin \theta \quad \text{and} \quad z = z. \tag{A-3}$$

The following transformation equations are obtained by applying the chain rule:

$$\frac{\partial}{\partial x} = \cos \theta \frac{\partial}{\partial r} - \frac{1}{r} \sin \theta \frac{\partial}{\partial \theta} , \tag{A-4}$$

$$\frac{\partial}{\partial y} = \sin \theta \frac{\partial}{\partial r} + \frac{1}{r} \cos \theta \frac{\partial}{\partial \theta} , \tag{A-5}$$

$$\frac{\partial}{\partial z} = \frac{\partial}{\partial z} . \tag{A-6}$$

Upon using equations A-4, A-5, and A-6 in equation A-2, the dissipative terms in rectangular coordinates become

$$\frac{\partial}{\partial x}\left(A\cos(\theta)\frac{\partial f}{\partial r}\right) - \frac{\partial}{\partial x}\left(\frac{A}{r}\sin(\theta)\frac{\partial f}{\partial \theta}\right) + \frac{\partial}{\partial y}\left(A\sin(\theta)\frac{\partial f}{\partial r}\right)$$

$$+ \frac{\partial}{\partial y}\left(\frac{A}{r}\cos(\theta)\frac{\partial f}{\partial r}\right) + \frac{\partial\left(A\frac{\partial f}{\partial z}\right)}{\partial z} . \qquad \text{(A-7)}$$

After substituting ($\sin^2\theta + \cos^2\theta = 1$) into equation (A-7) one obtains

$$\frac{\partial}{\partial r}\left(A\frac{\partial f}{\partial r}\right) + \frac{1}{r}\left(-\sin\theta\frac{\partial}{\partial\theta}\left(A\cos\theta\frac{\partial f}{\partial r}\right) + \frac{\sin\theta}{r}\frac{\partial}{\partial\theta}\left(A\sin\theta\frac{\partial f}{\partial\theta}\right)\right.$$

$$\left. + \cos\theta\frac{\partial}{\partial\theta}\left(A\sin\theta\frac{\partial f}{\partial r}\right) + \frac{\cos\theta}{r}\frac{\partial}{\partial r}\left(A\cos\theta\frac{\partial f}{\partial\theta}\right)\right) + \frac{\partial\left(A\frac{\partial f}{\partial z}\right)}{\partial z}$$

$$= \frac{\partial}{\partial r}\left(A\frac{\partial f}{\partial r}\right) + \frac{1}{r}\left(\sin^2\theta\, A\frac{\partial f}{\partial r} - \sin\theta\cos\theta\frac{\partial}{\partial\theta}\left(A\frac{\partial f}{\partial r}\right)\right.$$

$$+ \frac{\sin^2\theta}{r}\frac{\partial}{\partial\theta}\left(A\frac{\partial f}{\partial\theta}\right) + \frac{\sin\theta\cos\theta}{r}A\frac{\partial f}{\partial\theta} + \cos^2\theta\, A\frac{\partial f}{\partial r}$$

$$\left. + \cos\theta\sin\theta\frac{\partial}{\partial\theta}\left(A\frac{\partial f}{\partial r}\right) - \frac{\cos\theta\sin\theta}{r}A\frac{\partial f}{\partial\theta} + \frac{\cos^2\theta}{r}\frac{\left(A\frac{\partial f}{\partial r}\right)}{\partial\theta}\right)$$

$$- \frac{\partial\left(A\frac{\partial f}{\partial z}\right)}{\partial z} .$$

The above can be simplified by collecting terms to give

$$= \frac{\partial}{\partial r}\left(A\frac{\partial f}{\partial r}\right) + \frac{A}{r}\frac{\partial f}{\partial r} + \frac{1}{r^2}\frac{\partial}{\partial\theta}\left(A\frac{\partial f}{\partial\theta}\right) + \frac{\partial\left(A\frac{\partial f}{\partial z}\right)}{\partial z} ,$$

or

$$= \frac{1}{r}\frac{\partial}{\partial r}\left(rA\frac{\partial f}{\partial r}\right) + \frac{1}{r^2}\frac{\partial}{\partial\theta}\left(A\frac{\partial f}{\partial\theta}\right) + \frac{\partial\left(A\frac{\partial f}{\partial z}\right)}{\partial z} .$$

For axial symmetric systems $\frac{\partial}{\partial\theta}$ is identically zero; therefore, the dissipative terms for axial symmetric flows are

$$\frac{1}{r}\frac{\partial}{\partial r}\left(rB\frac{\partial f}{\partial r}\right) + \frac{\partial\left(A\frac{\partial f}{\partial z}\right)}{\partial z} . \qquad \text{(A-8)}$$

APPENDIX B

INITIAL CONDITIONS

Ideal Gas

The initial bow wave for ideal gas (Phase 1) was obtained by passing a normal shock over a body which had a relative zero velocity. Given below is the development of the equations which provide the initial data for Phase 1. The coordinate system for stationary shock is shown in Shock I.

Shock I

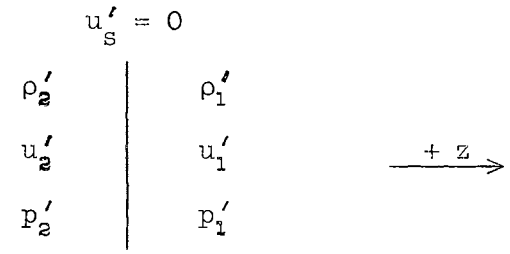

This stationary normal shock problem can be solved with the aid of ideal gas shock tables (reference 28). In order to obtain zero velocity on the right hand side of this shock, u_1' is superimposed in the positive z-direction.

Shock II

$$u_s = u_1'$$

$\rho_2 = \rho_2'$	$\rho_1 = \rho_1'$
$u_2 = u_1' - u_2'$	$u_1 = 0$
$p_2 = p_2'$	$p_1 = p_1'$

From Shock II the dimensionless velocity then becomes

$$U_2 = \frac{u_2}{\sqrt{\frac{p_1}{\rho_1}}} = \sqrt{\gamma}\,\frac{u_1' - u_2'}{\sqrt{\gamma\frac{p_1}{\rho_1}}} = \sqrt{\gamma}\left(\frac{u_1'}{\sqrt{\gamma\frac{p_1}{\rho_1}}} - \frac{u_2'}{\sqrt{\gamma\frac{p_2}{\rho_2}}\sqrt{\frac{\rho_2}{\rho_1}\frac{p_1}{p_2}}}\right)$$

$$= \sqrt{\gamma}\left(M_1' - M_2'\sqrt{\frac{p_2}{p_1}\frac{\rho_1}{\rho_2}}\right), \qquad \text{(B-1)}$$

and the free stream Mach number is derived to be

$$M_2 = U_2\sqrt{\sqrt{\gamma}\frac{p_2/p_1}{\rho_2/\rho_1}} \quad ,$$

where M_1' and M_2' are the Mach numbers on the low and high pressure sides, respectively, of a standing shock wave. It is noted that

$\frac{p_2}{p_1}$ = the dimensionless pressure on the left hand side of the shock, and

$\frac{\rho_2}{\rho_1}$ = the dimensionless density on the left hand side of the shock.

All of the parameters for Phase 1 are determined by selecting $\frac{p_2}{p_1}$.

Therefore, the dimensionless input data are:

$$RHO_2 = \frac{\rho_2}{\rho_1} \qquad RHO_1 = \frac{\rho_1}{\rho_1} = 1.0$$

$$ZM_2 = U_2 * RHO_2 \qquad ZM_1 = 0.0$$

and

$$RM_2 = 0.0 \qquad RM_1 = 0.0$$

$$P_2 = \frac{p_2}{p_1} \qquad P_1 = \frac{p_1}{p_1} = 1.0 \ .$$

After the initial bow wave is established (Phase 1), a new set of properties, representing the state of the air outside the blast front, is placed in the first column of mesh points. This blast or shock front will then propagate back over the cone (Figure 17).

To evaluate these properties, the normal shock (Figure 17) is transformed to coordinates, where $u_s' = 0$, by adding u_s to all velocities.

Shock III

$$u_s' = 0$$

$$\begin{array}{l|l} \rho_3' & \rho_2' \\ u_3' = -u_s + u_3 & u_2' = -u_s + u_2 \\ \quad = M_3'\sqrt{\gamma\frac{p_3'}{\rho_3}} & \quad = M_2'\sqrt{\gamma\frac{p_2}{\rho_2}} \\ p_3' & p_2' \end{array} \qquad \text{(B-2)}$$

This transformation allows the use of the normal shock tables to relate conditions on both sides of the shock. An expression for u_s is obtained from (B-2) as,

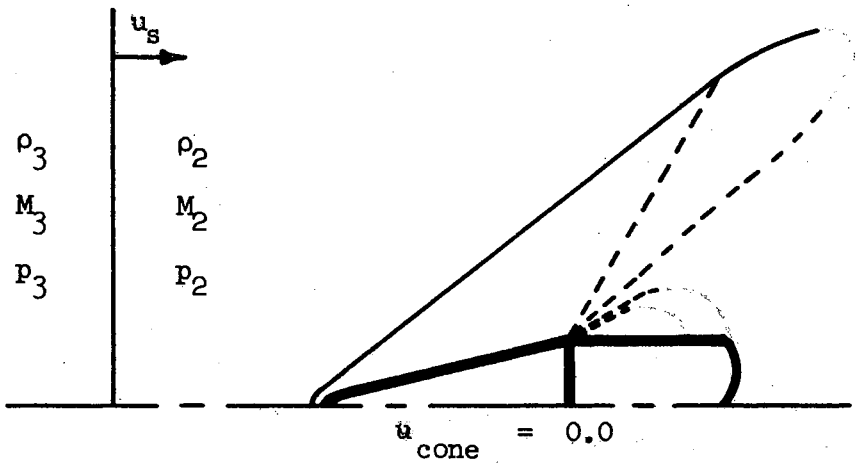

Figure 17. Initial Conditions for Phase 2

$$u_s = u_2 - M_2'\sqrt{\gamma\frac{p_2}{\rho_2}} \quad . \tag{B-3}$$

By solving (B-1) for u_3 the resulting expression is

$$u_3 = u_s + M_3'\sqrt{\gamma\frac{p_3}{\rho_3}} \quad . \tag{B-4}$$

Equation (B-3) can be used in (B-4) to give

$$u_3 = u_2 - M_2'\sqrt{\gamma\frac{p_2}{\rho_2}} + M_3'\sqrt{\gamma\frac{p_3}{\rho_3}} \quad , \text{ or}$$

$$u_3 = u_2 + \sqrt{\gamma}\left(M_3'\sqrt{\frac{p_3}{\rho_3}} - M_2'\sqrt{\frac{p_2}{\rho_2}}\right) .$$

The dimensionless velocity can be obtained as follows:

$$U_3 = \frac{u_2}{\sqrt{p_1/\rho_1}} + \sqrt{\gamma}\left(M_3'\sqrt{\frac{p_3/p_1}{\rho_3/\rho_1}} - M_2'\sqrt{\frac{p_2/p_1}{\rho_2/\rho_1}}\right),$$

$$U_3 = U_2 + \sqrt{\gamma}\left(M_3'\sqrt{\frac{(\frac{p_3}{p_2})(\frac{p_2}{p_1})}{(\frac{\rho_3}{\rho_2})(\frac{\rho_2}{\rho_1})}} - M_2'\sqrt{\frac{p_2/p_1}{\rho_2/\rho_1}}\right).$$

The free stream Mach number for Phase 2 is

$$M_3 = \frac{U_3}{\sqrt{\gamma}}\,\frac{\sqrt{(\frac{\rho_3}{\rho_2})(\frac{\rho_2}{\rho_1})}}{\sqrt{(\frac{p_3}{p_2})(\frac{p_2}{p_1})}} \quad .$$

The remaining required data, $(\frac{\rho_2}{\rho_1})$, M_3', M_2' can be obtained from NACA 1135 tables, by choosing a shock strength $(\frac{p_2}{p_3})$.

These data are:

$$RHO_3 = \frac{\rho_3}{\rho_2}\frac{\rho_2}{\rho_1},$$

$$ZM_3 = U_3 * RHO_3,$$

$$RM_3 = 0.0, \qquad \text{and}$$

$$P_3 = \frac{p_3}{p_2}\frac{p_2}{p_1}.$$

Real Gas

The initial Phase 2 free stream properties for the real gas case were chosen so that the dimensional velocity and dimensionless RHO and P were identical to those used for the ideal gas study. The proper reference values were discussed in Chapter III.

The pressure ratio across the Phase 2 shock for ideal and real gas case was also set equal. Using this given pressure ratio across a stationary shock, the corresponding values of $\frac{\rho_2}{\rho_1}$, u_3', and u_2', $\frac{p_2}{p_1}$, M_3, and $\frac{T_2}{T_1}$ can be obtained from "Normal Shock Wave Parameters in Equilibrium Air", (reference 29).

Shock IV

$$u_s' = 0$$

ρ_3'	ρ_2'
u_3'	u_2'
p_3'	p_2'

This coordinate system is then transformed so that u_1 is equal to the actual velocity in the ideal gas case: or

$u_3 = u_3' + vel = u_3$ (ideal gas), so

$u_2 = u_2' + vel$. The transformed coordinate system is

Shock V

$u_s = vel$

$\rho_3 = \rho_3'$	$\rho_2 = \rho_2'$
$u_3 = u_3' + vel$	$u_2 = u_2' + vel$
$p_3 = p_3'$	$p_2 = p_2'$.

The initial bow wave for Phase 1 real gas was obtained in the same manner as in the ideal gas case. For both the real and ideal gas cases the dimensionless properties in region two above were used along with

RHO = 1.0,

ZM = 0.0,

RM = 0.0 and

P = 1.0.

Entering Conditions for Real Gas

The steady-state condition for the second phase of the exiting case was used for the initial condition of the entering case. The conditions across the blast to be entered are obtained from reference 29 for a stationary shock:

$$u_s = 0$$

$$\begin{array}{c|c} \rho_4' & \rho_3' \\ u_4' & u_3' \\ p_4' & p_3' \end{array} .$$

The coordinate system is then transformed to make u_1 equal to the free stream velocity of Phase 2 of the exiting case:

$$\begin{array}{c|c} & u_s \\ \hline \rho_4 = \rho_4' & \rho_3 = \rho_3' \\ u_4 = -u_4' + u_s & u_3 = u_2 \\ p_4 = p_4' & p_3 = p_3' \end{array} .$$

The initial conditions used for Phase 3 are given in Figure 18.

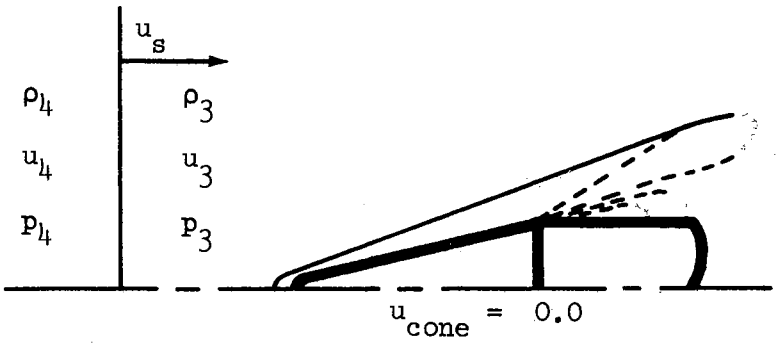

Figure 18. Initial Conditions for Phase 3

APPENDIX C

COMPUTER LOGIC DIAGRAM

The definitions of the terms used in the flow diagram are as follows:

I	one mesh point upstream from the nose
N	number of mesh points in z-direction
LMAX	number of mesh points in r-direction
NN	total number of time planes
NDEL	number of time planes between printouts
OMEG	defines amount of artificial damping
ALPO	defines time step
MSTAR	z-location of cone-cylinder intersection
RHO	density, n^{th} time plane, dimensionless
RHO1	density, $(n+1)^{th}$ time plane, dimensionless
ZM	mass flux in z-direction, n^{th} time plane, dimensionless
ZM1	mass flux in z-direction, $(n+1)^{th}$ time plane, dimensionless
RM	mass flux in r-direction, n^{th} time plane, dimensionless
RM1	mass flux in r-direction, $(n+1)^{th}$ time plane, dimensionless
P	pressure, n^{th} time plane, dimensionless
P1	pressure, $(n+1)^{th}$ time plane, dimensionless
EN	energy, n^{th} time plane, dimensionless
EN1	energy, $(n+1)^{th}$ time plane, dimensionless

J	counter - time planes between printouts
WC	local velocity modulus plus sonic velocity, dimensionless
WCMAX	maximum value of WC
TIME	running index of dimensionless time
ALP	coefficient of artificial viscosity in z-direction
BET	coefficient of artificial viscosity in r-direction
M	mesh point index in z-direction
L	mesh point index in r-direction
MM	index which keeps calculations above cone-cylinder surface
JJ	counter - total number of time planes

FLOW DIAGRAM

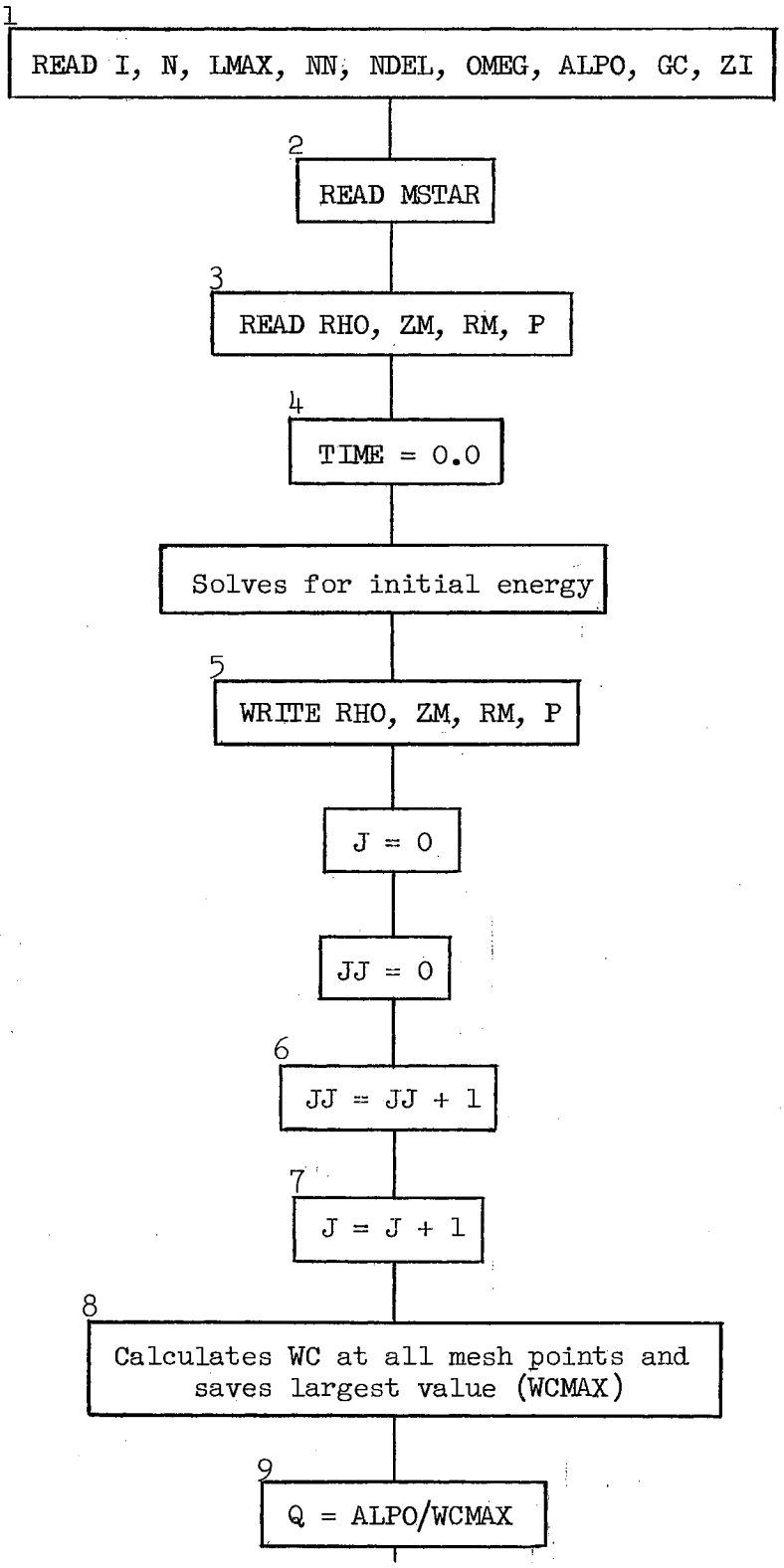

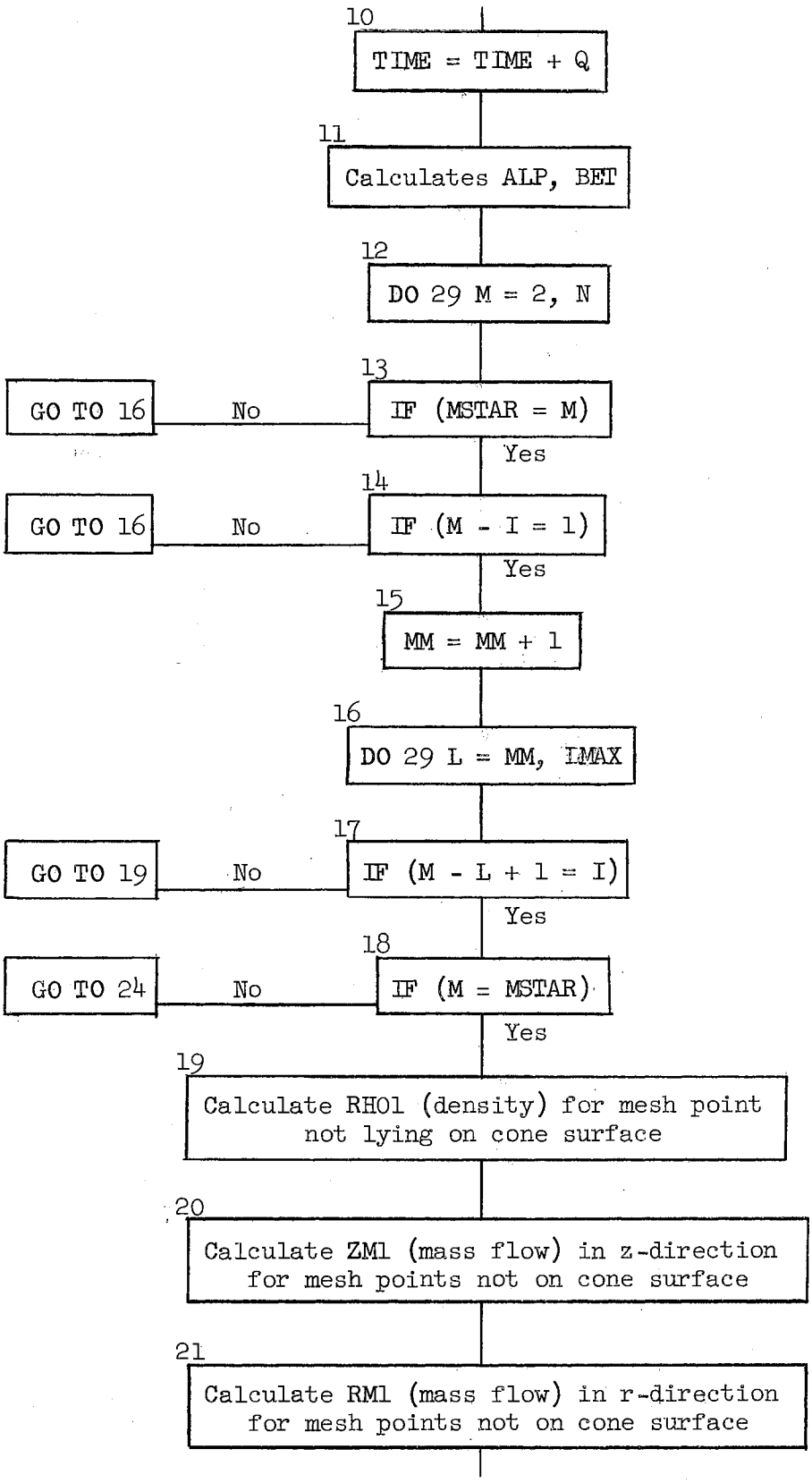
10
TIME = TIME + Q
11
Calculates ALP, BET
12
DO 29 M = 2, N
13
IF (MSTAR = M)
No
GO TO 16
Yes
14
IF (M - I = 1)
No
GO TO 16
Yes
15
MM = MM + 1
16
DO 29 L = MM, IMAX
17
IF (M - L + 1 = I)
No
GO TO 19
Yes
18
IF (M = MSTAR)
No
GO TO 24
Yes
19
Calculate RHO1 (density) for mesh point not lying on cone surface
20
Calculate ZM1 (mass flow) in z-direction for mesh points not on cone surface
21
Calculate RM1 (mass flow) in r-direction for mesh points not on cone surface

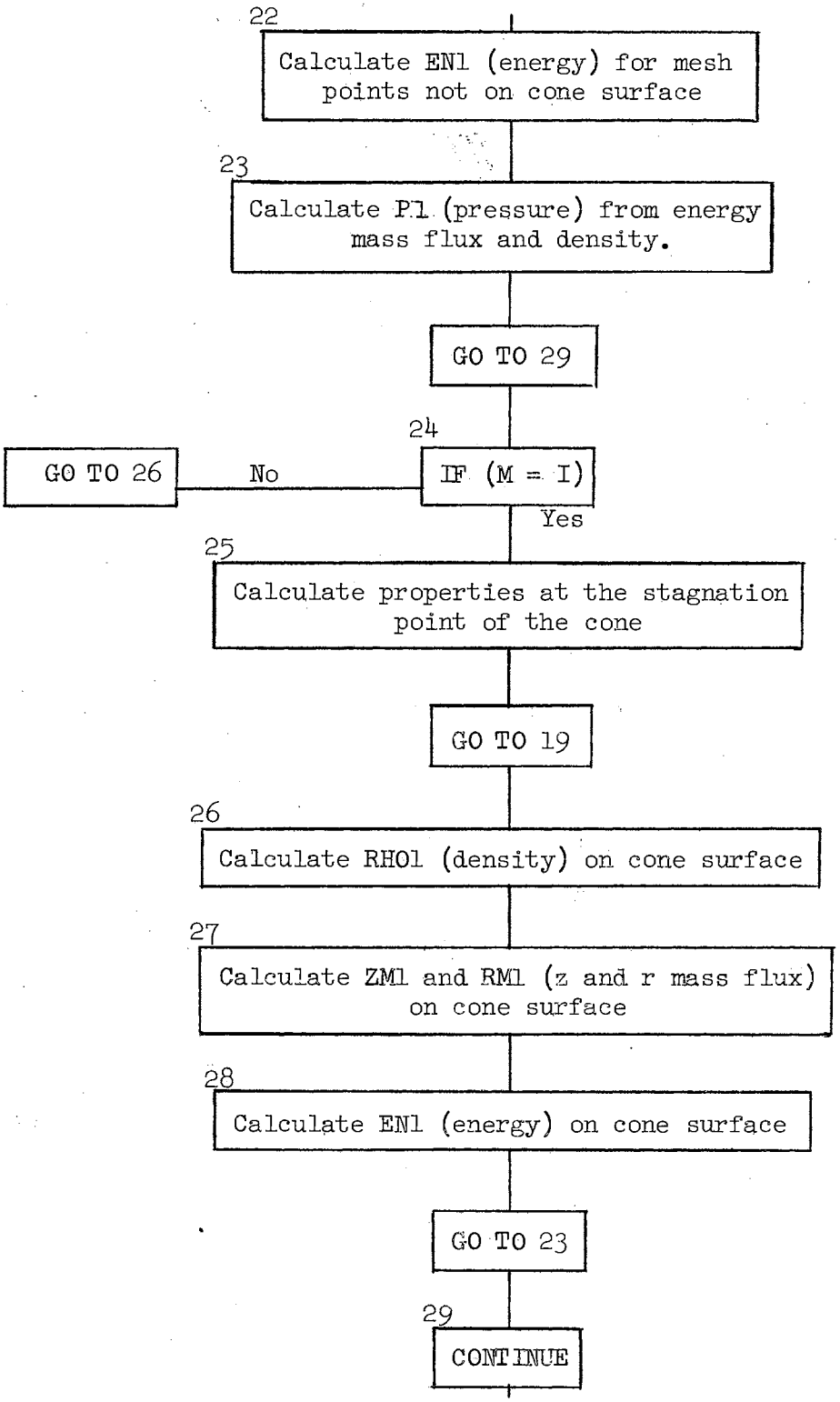

Comment: This completes the calculations for all mesh points at one time plane.

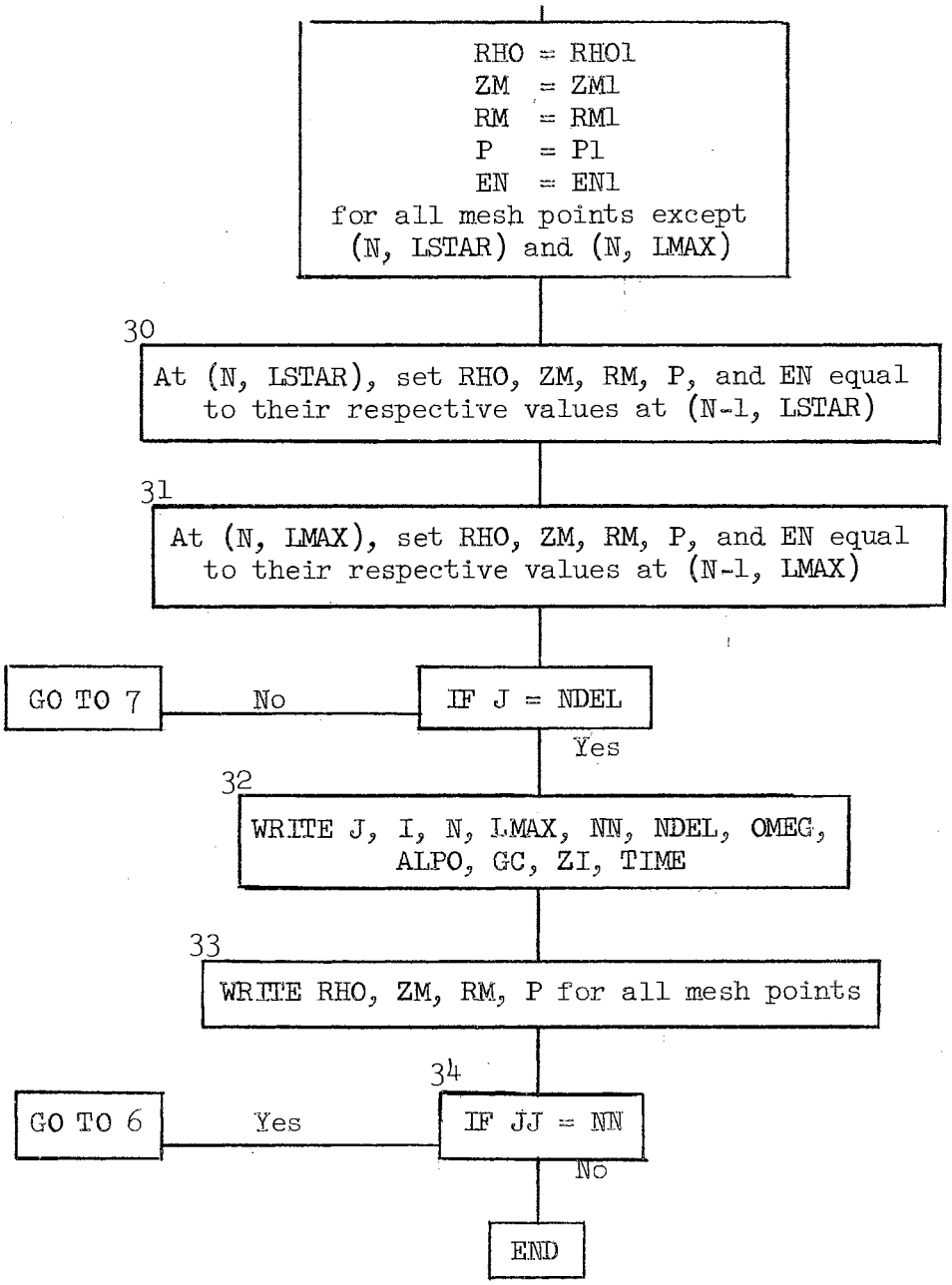
RHO = RHO1
ZM = ZM1
RM = RM1
P = P1
EN = EN1
for all mesh points except
(N, LSTAR) and (N, LMAX)
30
At (N, LSTAR), set RHO, ZM, RM, P, and EN equal to their respective values at (N-1, LSTAR)
31
At (N, LMAX), set RHO, ZM, RM, P, and EN equal to their respective values at (N-1, LMAX)
IF J = NDEL
No
GO TO 7
Yes
32
WRITE J, I, N, LMAX, NN, NDEL, OMEG, ALPO, GC, ZI, TIME
33
WRITE RHO, ZM, RM, P for all mesh points
34
IF JJ = NN
Yes
GO TO 6
No
END

VITA

Roger Ralph Eaton

Candidate for the Degree of

Doctor of Philosophy

Thesis: A NUMERICAL SOLUTION FOR THE FLOW FIELD OF A SUPERSONIC CONE-CYLINDER ENTERING AND LEAVING A BLAST SPHERE DIAMETRICALLY

Major Field: Mechanical and Aero Space Engineering

Biographical:

Personal Data: Born in Ellsworth, Kansas, June 15, 1937, the son of Ralph H. and Mary Lois Eaton.

Education: Attended grade school in Leoti and Kanopolis, Kansas; attended two years of high school at Hartford, Kansas and graduated from Randolph High School, Randolph, Kansas in 1956; received the Bachelor of Science degree in Mechanical Engineering from Kansas State University, Manhattan, Kansas in June, 1960; received the Master of Science degree from Kansas State University in June, 1962; completed the requirements for the Doctor of Philosophy degree in May, 1967.

Experience: Summer engineer for Boeing Aircraft, Wichita, Kansas during summer of 1959; Summer employee for D. C. Hoss Consulting Engineers, summer, 1960; Research Assistant for the School of Mechanical Engineering of Kansas State University, September, 1960 to June, 1962; Staff member at Sandia Corporation, Albuquerque, New Mexico, June, 1962 to September, 1964 and June, 1965 to September, 1965.

Professional Organizations: The author is a member of the following professional organizations: American Institute of Aeronautics and Astronautics, and American Society of Mechanical Engineers.